2

NO HEADING????

The FDTD method actively used at present to meet the challenges of nanophotonics [1, 2] has a long history. Appearing in the middle of the last century, [3] (G. Cron, 1944), the numerical method for solving Maxwell's equations has gone through several stages of development. Previously, only (S.K. Yee, 1966) [4] published explicit difference equations of a high order of approximation of the initial differential problem in time and space. Implicit finite difference schemes, characterized by absolute stability, were presented in 1997 [5] by D.L. Golovashkin, A.A. Degtyarev and V.I. Soifer, in 1998 [6] the same authors increased the order approximation in time for the implicit schemes, and in 2000 [7] also in space (Zheng, Chen, Zhang).

In 1994, J.–P. Berenger [8] satisfactorily solved the problem of numerical description of the absorption of radiation leaving the boundary of the computational domain.

The problem of modelling of the operation of the source of an incident wave, set by Yee in [4], has been solved with varying degrees of accuracy in many studies to date. The first way to specify the incident wave, which allows to limit the computational domain by the object under study and its immediate neighborhood, was formulated in the work [9] (A. Taflove, M. Brodwin, 1975). A more accurate method was published in 1980 [10] (A. Taflove) using the TF / SF technique (Total–Field/Scattering–Field technique). The increase in the accuracy of this approach in the region enclosed in a shell of a homogeneous medium, is described in a related work in 1999 [11] (D.W. Prather and S. Shi), in which the authors chose to define the emitting conditions numerically, rather than in the analytical form, as previously suggested in [10]. When finding an optical element in the shell of an inhomogeneous medium it is appropriate to apply the methodology of defining the incident wave, described further in section 2.1.4.

The computational complexity of the FDTD method is reduced by the imposition of a mobile grid area, as proposed in [12] (B. Fidel, E. Heyman, R. Kastner and R.W. Zioklowski). The specified method is well established in the study of short pulse propagation in a homogeneous medium. In section 2.1.5 a method is proposed for decomposing the grid domain, which reduces the computational complexity when modelling the propagation of monochromatic radiation.

The beam propagation method (BPM) was proposed in the 70s of XX century by Feit and Fleck [13] (M.D. Feit, 1978) and was designed for simulation and analysis of light propagation in waveguides with a gradient refractive index profile. Although originally the method was formulated in the framework of the scalar theory of light, and it aimed to the gradient media, the basic ideas and principles of the method are more fundamental and remain valid until now. This is confirmed, in particular, by a large number studies of the method that appeared in the last three decades, as well as studies in which the method is applied to solve research and applied problems.

Interesting also is the fact that a similar approach was independently proposed (and developed independently for a long period of time) in different fields of physics, namely in acoustics. There the method is called the parabolic equation method and is of considerable importance, for example, for the problems of hydroacoustics. At present, these methods are closely related, offer similar mathematical tools and, in fact, are almos identical. However, in some sense, the beam propagation method is more general, as it studies not only scalar cases.

The central idea of the beam propagation method is to reduce the order of differentiation with respect to the selected coordinate in the Helmholtz equation and subsequently solve the problem in the evolutionary form with respect to this coordinate. Feit and Fleck offered a fairly simple way to impose a number of very serious limitations on the scope of the method, but this solution has shown the principal possibility of such an approach.

Later on studies of the method aimed at overcoming its limitations. Thus, the beam propagation method, based on the method of lines, has made possible to perform simulations of light propagation in media with a more contrast refractive index profile [14] (J. Gerdes, 1991).

Further development of computer technology has made possible the effective use of finite–difference methods for solving the consequences of the Helmholtz equation which led to the emergence of a new family of the beam propagation methods (finite–difference BPM), removing a number of requirements for the field distribution in the propagating beam [15] (W. Huang, 1992). However, these methods are, in turn, limited as regards beam propagation: their application is incorrect if most of the energy is distributed at a considerable angle to the axis, considered as the main direction of propagation.

In turn, the application of the finite element approach and the more accurate approximations of differential operators allows us to relax the last restriction, which led to the emergence of yet another family of methods: methods of beam propagation for significant deviations in propagation (wide–angle BPM) [16, 17] (S.L. Chui, 2004 and Kh.Q. Le, 2009).

It should be noted that the studies, which set out the foundations of modern methods of beam propagation were mostly published in the early 90s of the twentieth century. Further development of the method occurred predominantly in the direction of improving the performance of the method through the use of more sophisticated mathematical tools and computational methods.

At present, the the beam propagation method is a rather large family of methods with different characteristics which determine which method is used for a specific

case. Together, these methods allow to solve a wide range of problems dealing with the propagation of radiation in dielectric media. The main limitations of the method and its mathematical foundations will be discussed in section 2.2.

2.1. Difference method for solving Maxwell's equations (FDTD–approach)

2.1.1. Explicit difference schemes for Maxwell's equations

The mathematical basis of the finite–difference time–domain method (FDTD method) are difference expressions for the Maxwell equations and the grid approximations of the boundary and initial conditions corresponding to the boundary value problems for the first and second kind and cyclic. Classical schemes by Yee [4] (from which the FDTD method is derived) allow the expression of each grid function via values of the functions values at the previous time layers explicitly. The main feature of these schemes is separate location of nodes of the grid area for each projection of the field strength. As shown in [7], this technique raises the order of approximation of the difference scheme of the initial boundary–value problem.

2.1.1.1. One–dimensional case

In the one–dimensional case with the Dirichlet boundary conditions on the area of computer simulation D^1 ($0 < t \leqslant T$, $0 \leqslant z \leqslant L_z$) we traditionally [4] D_h^1 superimpose a grid area in the nodes of which $\{(t_m, z_k)$: $t_m = mh_t$, $m = 0.1,..., M = T/h_t$, $z_k = kh_z$, $k = 0..., K = L_z/h_z\}$ we define the grid projection of the electric field on the axis X – $E_{x_k}^m$. The grid projection of the magnetic field on the axis Y – $H_{y_{k+0.5}}^{m+0.5}$ is defined at the nodes $\{(t_m + 0.5, z_{k+0.5})$: $t_{m+0.5} = (m + 0.5)\, h_t$, $m = 0.\ 1,\ ..,\ M - 1$, $z_{k+0.5} = (k + 0.5)\, h_z$, $k = 0,..., K - 1\}$. The index k varies in the range D_h^1 indicating the nodes in space, m – in time. Distances between nodes are given by the spatial (h_z) and time (h_t) grid steps. The grid value of of the dielectric constant (ε_k) characterizes the optical element being studied. Figure 2.1 presents the location of nodes D_h^1 in space, without taking into account the time coordinate.

Then Maxwell's equations in the one–dimensional case are usually written as the following difference analogue [4]:

$$\mu_0 \frac{H_{y_{k+0.5}}^{m+0.5} - H_{y_{k+0.5}}^{m-0.5}}{h_t} = -\frac{E_{x_{k+1}}^m - E_{x_k}^m}{h_z}; \tag{2.1}$$

$$\varepsilon_0 \varepsilon_k \frac{E_{x_k}^{m+1} - E_{x_k}^m}{h_t} = -\frac{H_{y_{k+0.5}}^{m+0.5} - H_{y_{k-0.5}}^{m+0.5}}{h_z}. \tag{2.2}$$

Figure 2.2 shows the differential pattern corresponding to (2.1) , (2.2).

By defining the Dirichlet boundary conditions for D_h^1 , we set

$$E_{x_0}^m = 0 \text{ and } E_{x_K}^m = 0 \ \%\% \ 0 \leq m \leq M. \tag{2.3}$$

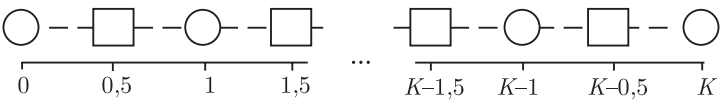

Fig. 2.1. Grid area D_h^1 without sampling over time. Circles correspond to the projection $E_{x_k}^m$, squares – $H_{y_{k+0,5}}^{m+0,5}$.

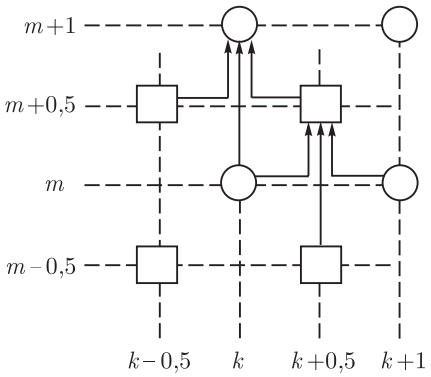

Fig. 2.2. The differential pattern for the construction of (2.1), (2.2). Circles correspond to the projection of the electric field $E_{x_k}^m$, the square – the magnetic field $H_{y_{k+0.5}}^{m+0.5}$.

The initial condition for D_h^1 written in

$$E_{x_k}^0 = \Phi_1(\mathrm{kh_z})\ (1 \le \mathrm{k} \le \mathrm{K}-1). \tag{2.4}$$

The grid projection of the magnetic field is not involved in the formation of the boundary and initial conditions in the field of view of the structure D_h^1, which does not provide for the location of nodes (t_m +0.5, z_k +0.5) at any of its border.

When setting the Neumann boundary condition we must be impose on D^1 the grid area $\bar{D}_h^1$ [18], in the nodes of which $\{(t_m, z_{k+0.5})$: $t_m = mh_t$, $m = 0.\ 1, .., M = T/h_t$, $z_k + 0.5 = (k+0.5)\ h_z$, $k = 1, .., K = L_z / h_z\}$ we define the grid projection of the electric field on the axis $X - E_{x_k+0.5}^m$. The grid projection of the magnetic field on the axis $Y - H_{y_K}^{m+0.5}$ is defined at the nodes $\{(t_{m+0.5}, z_k)$: $t_{m+0.5} = (m+0.5)\ h_t$, $m = 0.\ 1, .., M-1, z_k = kh_z$, $k = 0.\ .., K\}$. Figure 2.3 shows the location of nodes in space, without taking into account the time coordinate.

Redefining the grid area is associated with the imposition on the boundaries $z = 0$ and $z = L_z$ of the nodes of the magnetic field

$$H_{y_0}^{m+0.5} = 0 \ \text{ and } \ H_{y_K}^{m+0.5} = 0 \ \left(0 \le m \le M-1\right), \tag{2.5}$$

in contrast to the condition (2.3), which would entail the imposition on the boundaries of the nodes of the electric field. The initial condition for $\bar{D}_h^1$ is written in

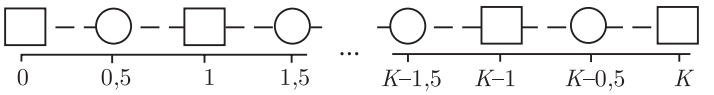

Fig. 2.3. Grid area D_h^1 without sampling over time. Circles correspond to the projection $E_{x_{k+0.5}}^m$, squares to $H_{y_k}^{m+0.5}$.

$$E^0_{x_{k+0.5}} = \Phi_1\left(\left(\mathrm{k}+0.5\right)\mathrm{h_z}\right) \ \left(0 \le \mathrm{k} \le \mathrm{K}-1\right). \quad \text{correct} \tag{2.6}$$

In this case, when writing the boundary conditions we do not use grid electric field strength, and write the initial condition without the magnetic field.

Then the difference analogue for the Maxwell's equations in the one-dimensional takes the form:

$$\mu_0 \frac{H^{m+0.5}_{y_k} - H^{m-0.5}_{y_k}}{h_t} = -\frac{E^m_{x_{k+0.5}} - E^m_{x_{k-0.5}}}{h_z}; \tag{2.7}$$

$$\varepsilon_0 \varepsilon_{k+0.5} \frac{E^{m+1}_{x_{k+0.5}} - E^m_{x_{k+0.5}}}{h_t} = -\frac{H^{m+0.5}_{y_{k+1}} - H^{m+0.5}_{y_k}}{h_z}. \tag{2.8}$$

Figure 2.4 shows a differential pattern corresponding to (2.7) (2.8).

Implementation of the cyclic boundary condition requires the imposition on D^1 of the grid area $\bar{D}^1_h$ (Fig. 2.5), in the nodes of which $\{(t_m, z_k)$: $t_m = mh_t$, $m = 0,..., M = T/h_t$, $z_k = kh_z$, $k = 0,..., K-1$ $(K = L_z/h_z)\}$ we define the grid projection of the electric field on the axis $X - E^m_{x_k}$. The grid projection of the magnetic field on the axis $Y - H^{m+0.5}_{y_k+0.5}$ is defined at the nodes $\{(t_m + 0.5, z_{k+0.5})$: $t_{m+0.5} = (m + 0.5)\, h_t$, $m = 0.\ 1,..., M-1$, $z_{k+0.5} = (k + 0.5)\, h_z$, $k = 0,..., K-1\}$.

In contrast to D^1_h, the region $\tilde{D}^1_h$ does not contain a node for $E^m_{x_k}$ because of its redundancy, since the cyclic condition implies the equality of the field strengths at $z = 0$ and $z = L_z$. The difference equations in solving Maxwell's equations coincide with the previously submitted equations, except for the node $k = 0$ (for the definition of the electric field) and $k = K-1$ (for the definition of the magnetic field). For them is true:

$$\mu_0 \frac{H^{m+0.5}_{y_{K-0.5}} - H^{m-0.5}_{y_{K-0,5}}}{h_t} = -\frac{E^m_{x_0} - E^m_{x_{K-1}}}{h_z}; \tag{2.9}$$

$$\varepsilon_0 \varepsilon_k \frac{E^{m+1}_{x_0} - E^m_{x_0}}{h_t} = -\frac{H^{m+0.5}_{y_{0.5}} - H^{m+0.5}_{y_{K-0.5}}}{h_z}. \tag{2.10}$$

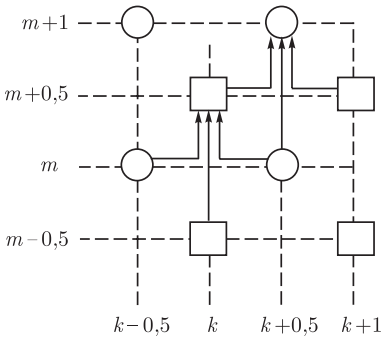

Fig. 2.4. The differential pattern for the construction of (2.7), (2.8). Circles correspond to the projection of the electric field $E^m_{x_{k+0.5}}$, the square – the magnetic field $H^{m+0.5}_{y_k}$.

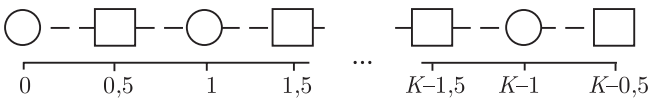

Fig. 2.5. Grid area without sampling over time. Circles correspond to the projection $E^{m}_{x_k}$, squares – $H^{m+0.5}_{y_{k+0.5}}$.

The initial condition $\tilde{D}^1_h$ is written as $E^0_{x_k} = \Phi_1(kh_z)$ $(0 \le k \le K-1)$.

Computational procedures, associated with the proposed schemes, are based on the alternation of time layers: the grid function at the next time step can be expressed solely in terms of functions in the previous two layers (the property of explicit difference schemes). Thus, equations (2.1)–(2.2) are conveniently solved in the form of

$$\text{correct} \qquad \mathrm{H}^{\mathrm{m+0.5}}_{\mathrm{y_{k+0.5}}} = \mathrm{H}^{\mathrm{m-0.5}}_{\mathrm{y_{k+0.5}}} - \frac{\mathrm{h_t}}{\mu_0 \mathrm{h_z}}\left(\mathrm{E}^{\mathrm{m}}_{\mathrm{x_{k+1}}} - \mathrm{E}^{\mathrm{m}}_{\mathrm{x_k}}\right); \tag{2.11}$$

$$E^{m+1}_{x_k} = E^{m}_{x_k} - \frac{h_t}{\varepsilon_0 \varepsilon_k h_z}\left(H^{m+0.5}_{y_{k+0.5}} - H^{m+0.5}_{y_{k-0.5}}\right), \tag{2.12}$$

and (2.7) – (2.8) is rewritten as

$$H^{m+0.5}_{y_k} = H^{m-0.5}_{y_k} - \frac{h_t}{\mu_0 h_z}\left(E^{m}_{x_{k+0.5}} - E^{m}_{x_{k-0.5}}\right); \tag{2.13}$$

$$E^{m+1}_{x_{k+0.5}} = E^{m}_{x_{k+0.5}} - \frac{h_t}{\varepsilon_0 \varepsilon_{k+0.5} h_z}\left(H^{m+0.5}_{y_{k+1}} - H^{m+0.5}_{y_k}\right). \tag{2.14}$$

Accordingly, (2.9) and (2.10) take the form

$$H^{m+0.5}_{y_{K-0.5}} = H^{m-0.5}_{y_{K-0.5}} - \frac{h_t}{\mu_0 h_z}\left(E^{m}_{x_0} - E^{m}_{x_{K-1}}\right); \tag{2.15}$$

$$E^{m+1}_{x_0} = E^{m}_{x_0} - \frac{h_t}{\varepsilon_0 \varepsilon_k h_z}\left(H^{m+0.5}_{y_{0.5}} - H^{m+0.5}_{y_{K-0.5}}\right). \tag{2.16}$$

The advantage of algorithms for solving (2.11)–(2.14) is the possibility of vectorization. Calculations for a time step of (2.11) – (2.13) can be expressed through a single operation of vector addition of the electric field and a single operation saxpy [19] (triad [20]) with a scalar $-\frac{h_t}{\mu_0 h_z}$. For (2.12), (2.14) after the addition of vectors of the magnetic field and in front of saxpy with $-\frac{h_t}{\varepsilon_0 h_z}$ we add a component-wise operation dividing the result of addition by the vector of values of ε_k where $1 \le k \le K-1$ for (2.14) or $\varepsilon_{k+0.5}$, where $0 \le k \le K-1$ for (2.14)

It is known that the difference scheme (2.1)–(2.4) approximates the initial differential problem with the order $O\left(h_t^2, h_z^2\right)$ and stable [21] provided $\frac{h_t}{h_z} \le \frac{1}{c} O\left(h_t^2, h_z^2\right)$

[9] (c is the speed of light in the medium). It is obvious that the other two schemes: (2.5)–(2.8) and (2.1), (2.2), (2.4), (2.9) and (2.10) are characterized by the same order of approximation and the stability condition, as derived from (2.1)–(2.4) modifications of the grid area. Shifting in the pattern in Fig. 2.4 the writing below the vertical dashed lines to the right by one position, we obtain the pattern shown in Fig. 2.2.

2.1.1.2. The two–dimensional case

On the two–dimensional area of computer simulation D^2 ($0 < t \le T$, $0 \le y \le L_y$, $0 \le z \le L_z$) we traditionally [4] superimpose the grid area in which the nodes D_h^2, $\{(t_m, y_j, z_k)$: $t_m = mh_t$, $m = 0.\ 1, .., M = T / h_t$, $y_j = jh_y$, $j = 0, .., J = L_y / h_y$, $z_k = kh_z$, $k = 0,..., K = L_z / h_z\}$ define the grid projection of the electric field on the axis X –???. The grid projection of the magnetic field on the axis $Z - H_{y_j+0.5,k}^{m+0.5}$ is define at the nodes $\{(t_{m+0.5}, y_{j+0.5}, z_k)$: $t_{m+0.5} = (m+0.5)\, h_t$, $m = 0.\ 1,..., M–1$, $y_{j+0.5} = (j+0.5)\, h_y$, $j = 0,..., J–1$, $z_k = kh_z$, $k = 1, .., K–1\}$ and the projection of the magnetic field at $Y - H_{y_{j,k+0.5}}^{m+0.5}$. at the nodes $\{(t_{m+0.5}, y_j, z_{k+0.5})$: $t_{m+0.5} = (m+0.5)\, h_t$, $m = 0.\ 1,..., M-1$, $y_j = jh_y$, $j = 1,..., J–1$, $z_{k+0.5} = (k+0.5)\, h_z$, $k = 0,..., K–1\}$. Figure 2.6 presents the location of nodes D_h^2 in space, without taking into account the time coordinate.

In the proposed area the indices j, k denote the nodes in space (directions Y and Z), m – in time. Distances between nodes are given by the spatial (h_y and h_z) and time (h_t) grid steps. The grid value of the dielectric constant ($\varepsilon_{j,k}$) characterizes the optical element being studied.

The system (2.1), (2.4) in the two-dimensional case for the TE wave is then usually written in the following difference analogue [4] :

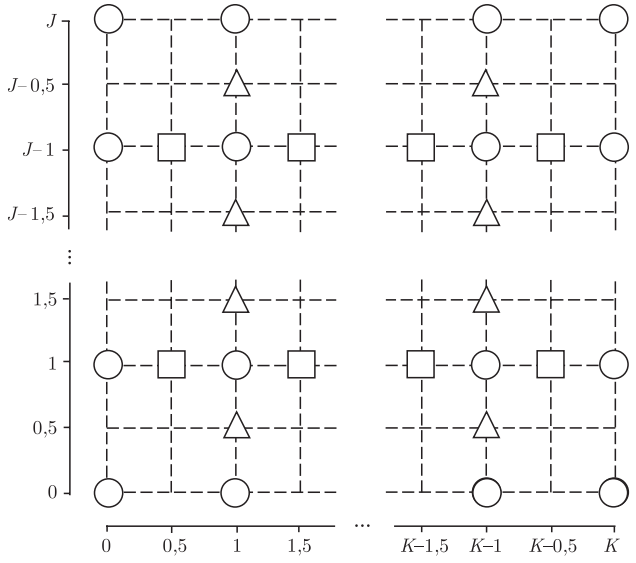

Fig. 2.6. Grid area D_h^2 without sampling over time. Circles correspond to the projections $E_{x_{j,k}}^m$ triangles – $H_{z_j+0.5}\, k^{m+0.5}$, squares – $H_{y_{j,\,k+0.5}}^{m\,+0.5}$.

$$\mu_0 \frac{H_{y_{j,k+0.5}}^{m+0.5} - H_{y_{j,k+0.5}}^{m-0.5}}{h_t} = -\frac{E_{x_{j,k+1}}^{m} - E_{x_{j,k}}^{m}}{h_z}; \tag{2.17}$$

$$\mu_0 \frac{H_{z_{j+0.5,k}}^{m+0.5} - H_{z_{j+0.5,k}}^{m-0.5}}{h_t} = \frac{E_{x_{j+1,k}}^{m} - E_{x_{j,k}}^{m}}{h_y}; \tag{2.18}$$

$$\varepsilon_0 \varepsilon_{j,k} \frac{E_{x_{j,k}}^{m+1} - E_{x_{j,k}}^{m}}{h_t} = \frac{H_{z_{j+0.5,k}}^{m+0.5} - H_{z_{j-0.5,k}}^{m+0.5}}{h_y} - \frac{H_{y_{j,k+0.5}}^{m+0.5} - H_{y_{j,k-0.5}}^{m+0.5}}{h_z}. \tag{2.19}$$

By defining D_h^2 for the Dirichlet boundary conditions, we set

$$\begin{aligned} &E_{x_{0,k}}^{m} = 0 \quad E_{x_{J,k}}^{m} = 0 \qquad 0 \le \mathrm{m} \le M \quad 0 \le \mathrm{k} \le K; \\ &E_{x_{j,0}}^{m} = 0 \quad E_{x_{j,K}}^{m} = 0 \qquad 0 \le \mathrm{m} \le M \quad 0 \le \mathrm{j} \le J. \end{aligned} \tag{2.20}$$

The initial condition for D_h^2 is written as

$$D_h^2 = \Phi_2\left(\mathrm{jhy}, \mathrm{khz}\right) \ \left(1 \le \mathrm{j} \le \mathrm{J}-1, \ 1 \le \mathrm{k} \le \mathrm{K}-1\right). \tag{2.21}$$

Grid projections of the magnetic field do not participate in the formation of boundary and initial conditions because of the structure of the region D_h^2, and do not lead to the location of nodes $(t_{m+0.5}, y_j, z_{k+0.5})$ and $(t_{m+0.5}, y_{j+0.5}, z_k)$ at any of its boundaries(Fig. 2.6).

When setting the Neumann boundary condition we must imposed on grid D^2 the domain $\bar{D}_h^1$ (Fig. 2.7) [18], in the nodes of which $\{(t_m, y_{j+0.5}, z_{k+0.5})$: $t_m = mh_t$, $m = 0.\ 1, .., M = T / h_t$, $y_{j+0.5} = (j+0.5)\, hy$, $j = 0. .., J–1$ $(J = L_y / h_y)$, $z_{k+0.5} = (k + 0.5)h_z$, $k = 0. .., K–1$ $(K = L_z / h_z)\}$ defined the grid projection of the electric field on the axis $X-$ $E_{x_{j+0.5,k+0.5}}^{m}$. The grid projection of the magnetic field on the axis $Z-$ $H_{z_{j,k+0.5}}^{m+0.5}$ is defined at the nodes $\{(t_{m+0.5}, y_j, z_{k+0.5})$: $t_{m+0.5} = (m+0.5)\, h_t$, $m = 0.\ 1,.., M–1$, $y_j = jh_y$, $j = 0. .., J$, $z_{k+0.5} = (k+0.5)\, h_z$, $k = 0. .., K–1\}$ and the projection of the magnetic field on the $Y-$ $H_{y_{j+0.5,k}}^{m+0.5}$ at the nodes $\{(t_{m+0.5}, y_{j+0.5}, z_k)$: $t_{m+0.5} = (m+0.5)\, h_t$, $m = 0.\ 1, .., M–1$, $y_{j+0.5} = (j+0.5)\, h_y$, $j = 0. .., J–1$, $z_k = kh_z$, $k = 0. .., K\}$.

Redefining the grid area associated with the imposition of limits on the boundaries $z = 0$ and $z = L_z$, the nodes for $H_{y_{j+0.5,k}}^{m+0.5}$, and at $y = 0$ and $y = L_y$ the nodes for $H_{z_{j,k+0.5}}^{m+0.5}$:

$$\begin{aligned} &H_{y_{j+0.5.\ 0}}^{m+0.5} = 0 \ \text{ and } \ H_{y_{j+0.5,\,K}}^{m+0.5} = 0 \ \text{ at } \ 0 \le m \le M-1 \ \text{ and } \ 0 \le j \le J-1; \\ &H_{z_{0,\,k+0.5}}^{m+0.5} = 0 \ \text{ and } \ H_{z_{J,k+0.5}}^{m+0.5} = 0 \ \text{ at } \ 0 \le m \le M-1 \ \text{ and } \ 0 \le k \le K-1 \end{aligned} \tag{2.22}$$

in contrast to the condition (2.20), which would entail the imposition of the nodes of the electric field on the boundaries. The initial condition $\bar{D}_h^1$ is written in

$$E_{x_{j+0.5,\,k+0.5}}^{0} = \Phi_2\left(\left(\mathrm{j}+0.5\right)\mathrm{h_y}, \left(\mathrm{k}+0.5\right)\mathrm{h_z}\right) \ \left(0 \le \mathrm{j} \le \mathrm{J}-1, \ 0 \le \mathrm{k} \le \mathrm{K}-1\right). \tag{2.23}$$

In this case, when writing the boundary conditions we do not use the grid strength of electric field, and in writing the initial condition the magnetic field is not considered.

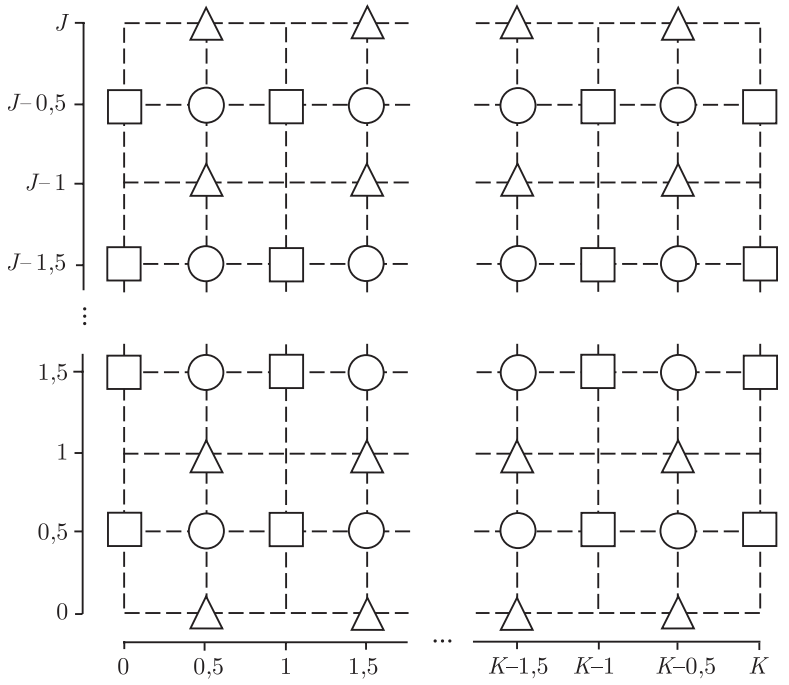

Fig. 2.7. Grid area $\bar{D}_h^2$ without sampling over time. Circles correspond to the projections, triangles – $H_{z_{j,k+0.5}}^{m+0.5}$, squares – $H_{y_{j+0.5,k}}^{m+0.5}$.

Then the system (2.7) (2.8) in the case study of the TE wave is usually written as the following difference analogue [18]:

$$\mu_0 \frac{H_{y_{j+0.5,\,k}}^{m+0.5} - H_{y_{j+0.5,\,k}}^{m-0.5}}{h_t} = -\frac{E_{x_{j+0.5,\,k+0.5}}^{m} - E_{x_{j+0.5,\,k-0.5}}^{m}}{h_z}; \tag{2.24}$$

$$\mu_0 \frac{H_{z_{j,\,k+0.5}}^{m+0.5} - H_{z_{j,\,k+0.5}}^{m-0.5}}{h_t} = \frac{E_{x_{j+0.5,\,k+0.5}}^{m} - E_{x_{j-0.5,\,k+0.5}}^{m}}{h_y}; \tag{2.25}$$

$$\varepsilon_0 \varepsilon_{j+0.5,\,k+0.5} \frac{E_{x_{j+0.5,\,k+0.5}}^{m+1} - E_{x_{j+0.5,\,k+0.5}}^{m}}{h_t} = \frac{H_{z_{j+1,\,k+0.5}}^{m+0.5} - H_{z_{j,\,k+0.5}}^{m+0.5}}{h_y} - \frac{H_{y_{j+0.5,\,k+1}}^{m+0,5} - H_{y_{j+0.5,\,k}}^{m+0,5}}{h_z}. \tag{2.26}$$

Implementation of the cyclic boundary condition requires the imposition on D^2 of the grid domain $\tilde{D}_h^2$ (Fig. 2.8), in the nodes of which $\{(t_m, y_j, z_k)$: $t_m = mh_t$, $m = 0.\ 1, .., M = T / h_t$, $y_j = jh_y$, $j = 0. .., J–1$ $(J = L_y / h_y)$, $z_k = kh_z$, $k = 0. .., K–1$ $(K = L_z / h_z)\}$ we define the grid projection of the electric field on the axis X – E???. The grid projection of the magnetic field on axis Z – $H_{z_{j+0.5,k}}^{m+0.5}$ is defined at the nodes $\{(t_{m+0.5}, y_{j+0.5}, z_k)$: $t_{m+0.5} = (m+0.5)\, h_t$, $m = 0.\ 1, .., M–1$, $y_{j+0.5} = (j+0.5)\, h_y$, $j = 0. .., J–1$, $z_k = kh_z$, $k = 0. .., K–1\}$ and the projection of the magnetic field on Y – $H_{y_{j,k+0.5}}^{m+0.5}$ at the

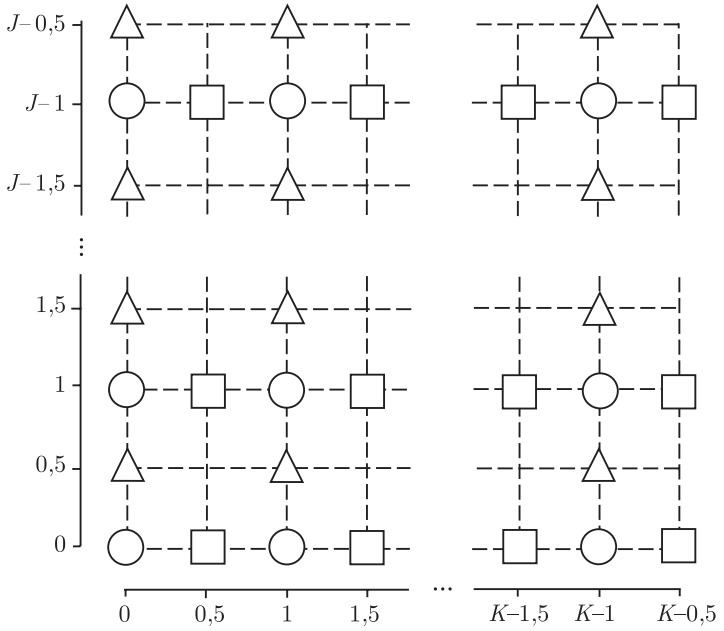

Fig. 2.8 Grid area $\tilde{D}_h^1$ without sampling over time. Circles correspond to the projections, triangles – $H_{z_{j+0.5,\,k}}^{m\,+0.5}$, squares – $H_{y_{j,k+0.5}}^{m\,+0.5}$.

nodes $\{(t_{m+0.5}, y_j, z_{k+0.5})$: $t_{m+0.5} = (m + 0.5)\, h_t$, $m = 0.\ 1, .., M–1$, $y_j = jh_y$, $j = 0. .., J–1$, $z_{k+0.5} = (k + 0.5)\, h_z$, $k = 0. .., K–1\}$.

In contrast to D_h^2, the region $\tilde{D}_h^2$ does not contain nodes for ??? ($0 \le j \le J$) and ($0 \le k \le K$), due to their redundancy, because the cyclic condition implies the equality of the field strengths at the opposite boundaries. In addition, on $\tilde{D}_h^2$ there were additional sites for ($0 \le j \le J - 1$) and ($0 \le k \le K–1$) used in the definition of the electric field which previously defined the electrical wall on $\tilde{D}_h^2$.

Recording of difference equations with cyclic boundary conditions coincides with (2.17) – (2.19) with the following exceptions. Instead of (2.17) for $0 \le j \le J–1$, we have

$$\mu_0 \frac{H_{y_{j,K-0.5}}^{m+0.5} - H_{y_{j,K-0.5}}^{m-0.5}}{h_t} = -\frac{E_{x_{j,0}}^{m} - E_{x_{j,K-1}}^{m}}{h_z}. \tag{2.27}$$

Further, (2.18) at $0 \le k \le K–1$ takes the form

$$\mu_0 \frac{H_{z_{J-0.5,k}}^{m+0.5} - H_{z_{J-0.5,k}}^{m-0.5}}{h_t} = \frac{E_{x_{0,k}}^{m} - E_{x_{J-1,k}}^{m}}{h_y}. \tag{2.28}$$

For (2.19) at $1 \le j \le J - 1$, we have

$$\varepsilon_0 \varepsilon_{j,0} \frac{E_{x_{j,0}}^{m+1} - E_{x_{j,0}}^{m}}{h_t} = \frac{H_{z_{j+0.5.0}}^{m+0.5} - H_{z_{j-0.5.0}}^{m+0.5}}{h_y} - \frac{H_{y_{j,\,0.5}}^{m+0.5} - H_{y_{j,K-0.5}}^{m+0.5}}{h_z}, \tag{2.29}$$

for $1 \le k \le K$–1

$$\varepsilon_0 \varepsilon_{0,k} \frac{E_{x_{0,k}}^{m+1} - E_{x_{0,k}}^{m}}{h_t} = \frac{H_{z_{0.5,k}}^{m+0.5} - H_{z_{J-0.5,k}}^{m+0.5}}{h_y} - \frac{H_{y_{j,k+0.5}}^{m+0.5} - H_{y_{j,k-0.5}}^{m+0.5}}{h_z}. \qquad (2.30)$$

and for the node $j = 0$, $k = 0$

$$\varepsilon_0 \varepsilon_{0,0} \frac{E_{x_{0.0}}^{m+1} - E_{x_{0.0}}^{m}}{h_t} = \frac{H_{z_{0.5.\,0}}^{m+0.5} - H_{z_{J-0.5.\,0}}^{m+0.5}}{h_y} - \frac{H_{y_{0.\,0.5}}^{m+0.5} - H_{0_{0,J-0.5}}^{m+0.5}}{h_z}. \qquad (2.31)$$

The initial condition for $\tilde{D}_h^2$ is formed as $E_{x_{j,k}}^0 = \Phi_2\,(jh_y,\, kh_z)$ $(0 \le j \le J$–1, $0 \le k \le K$–1).

Shifting to the right side of (2.17) – (2.19) (2.24) – (2.26) and (2.27) – (2.31), all grid functions defined on the previous time layers, we obtain the computational procedure for calculating the fields shown on the three schemes.

Vectorization of such procedures is associated with recording of row- or column-oriented algorithms [22] (depending on the method of storing the matrix in the computer memory) that shortens the duration searching the computer memory [19]. Recording of the vector algorithms in two-dimensional case is very important because of the high computational complexity of the given procedures. We write down the fields in the computer memory in the form of matrices (two-dimensional arrays), the first index of which points to a line, the second to a column. For definiteness, we set the first index j (corresponding to the direction Y in the grid areas), the second k (direction Z).

When storing the fields in the above manner by columns (for example, in using the language Fortran) computations by (2.17) and (2.24) are accompanied by operations of calculation of K and K–1 vectors $H_{y_{j,k+0.5}}^{m+0.5}$ $(1 \le j \le J$–1) and $H_{y_{i+0.5,k}}^{m+0.5}$ $(0 \le j \le J$ –1), respectively. Each operation in the calculation of the values of this vector consists of vector addition and subsequent saxpy. The scalar in saxpy is equal $-h_t / h_z \mu_0$, and the length of the resulting vectors is $J - 1$ in the calculation by (2.17) and J by (2.24).

Calculations using (2.18) and (2.25) involve performing operations with the calculation of the K–1 and K vectors $H_{z_{j+0.5,k}}^{m+0.5}$ $(0 \le j \le J$–1) and $H_{z_{j,k+0.5}}^{m+0.5}$ $(1 \le j \le J$–1), respectively. As in the previous case, each operation of the calculation of the values of this vector consists of vector addition and subsequent saxpy. The scalar in saxpy equals $-h_t / h_y \mu_0$, and the length of the resulting vectors is J in the computation by (2.18) and J–1 by (2.25).

Similarly, referring to the calculation using (2.19) and (2.26), one should bear in mind the calculation of the K–1 and K vectors $E_{x_{j,k}}^{m+1}$ $(1 \le \mathrm{j} \le J$–1) and $E_{x_{j+0.5,\,k+0.5}}^{m+1}$ $(0 \le j \le J$–1) the length J–1 and J. At the same time, to form each vector, we require two vector additions of the grid components of the magnetic field H_y and H_z (the vectors of the same projection are added), two component-wise divisions of the results of these additions to the value of the vector $\varepsilon_{j,k}$ $(1 \le j \le J$–1) for (2.19) and $\varepsilon_{k+0.5,j+0.5}$ $(0 \le j \le J$–1) for (2.26), two multiplications of the resulting vectors by scalars $ht/\varepsilon_0 h_y$ and ??? . Then the resulting vectors are added with each other and with the vector ??? $(1 \le j \le J$–1) in the calculation by (2.19) and $E_{x_{j+0.5,\,k+0.5}}^{m}$ $(0 \le j \le J$–1) in the calculation by (2.26).

In the case where $J < K$, the row-oriented algorithms [19] are preferable to column-oriented as they permit operations with vectors of greater length, providing a better loading of the conveyor???.

When storing the fields in two-dimensional arrays of lines (for example, in using the language C) calculations using (2.17) and (2.24) are accompanied by operations of the calculation of J–1 and J vectors $H^{m+0.5}_{y_{j,k+0.5}}$ $(0 \le k \le K–1)$ and $H^{m+0.5}_{y_{j+0.5,k}}$ $(1 \le k \le K–1)$, respectively. Each operation of the calculation of the values of this vector consists of vector addition and subsequent saxpy. The scalar in saxpy is equal to $-\frac{h_t}{h_z \mu_0}$, and the length of the resulting vector is K in the calculation of (2.17) and K–1 in the case of (2.24).

Implementation of calculations by (2.18) and (2.25) involves performing operations of the calculation of J and J–1 vectors $H^{m+0.5}_{z_{j+0.5,k}}$ $(1 \le k \le K–1)$ and $H^{m+0.5}_{z_{j,k+0.5}}$ $(0 \le k \le K–1)$, respectively. As in the previous case, each operation of the calculation of the values of this vector consists of vector addition and subsequent saxpy. The scalar in saxpy is equal to $\frac{h_t}{h_y \mu_0}$, and the length of the resulting vectors is K–1 in the calculation of (2.18) and K in (2.25).

Similarly, referring to the calculation of (2.19) and (2.26), one should bear in mind the calculation of the J–1 and J vectors $E^{m+1}_{x_{j,k,}}$ $(1 \le j \le J–1)$ and $E^{m+1}_{x_{j+0.5,\,k+0.5}}$ $(0 \le j \le J–1)$ with length K–1 and K. At the same time, to form each vector, we require two vector addition of the grid component of the magnetic field H_y and H_z (the vectors of one projection are added), two component-wise division of the results of these additions by the value of the vector $\varepsilon_{j,\,k}$ $(1 \le j \le J–1)$ for (2.19) and $\varepsilon_{k+0.5,\,j+0.5}$ $(0 \le j \le J–1)$ for (2.26), and two multiplications of the resulting vectors by scalars $\frac{h_t}{\varepsilon_0 h_y}$ and $-\frac{h_t}{\varepsilon_0 h_z}$. The resulting vectors are then added with each other and with the vector $E^{m}_{x_{j,k}}$ $(1 \le j \le J–1)$ in the calculation by (2.19) and $E^{m}_{x_{j+0.5,\,k+0.5}}$ $(0 \le j \le J–1)$ in the calculation by (2.26).

Do not assume that the shape of the investigated optical element determines imperatively the choice of the algorithmic programming language. This means that in the study of radiation passing through the DOE, elongated along the axis Y, it is appropriate to implement exclusively column-oriented algorithms. In contrast, in the study of optical elements, extending along the axis Z, is reasonable to use only row-oriented methods. In fact, the researcher is free to use any form of writing (row or column-oriented), changing the direction of the axes and rewriting if necessary the difference equations in the new coordinate system.

Of separate interest are block algorithms – the most efficient way to operate with the cache memory of the computer [19]. Their implementation is associated with the storage of fields in two-dimensional arrays of blocks, which requires the development of algorithms for writing (and reading) the values of network

functions in the computer memory which from the standard row- or column-oriented functions.

It is known that the difference scheme (2.17)–(2.21) approximates the initial differential problem with the order $O(h_t^2, h_y^2, h_z^2)$ and is stable under the condition $h_t \sqrt{\frac{1}{h_y^2} + \frac{1}{h_z^2}} \le \frac{1}{c}$ [9]. It is obvious that the other two schemes (2.22) – (2.26) and (2.17) – (2.19) (2.27) – (2.31) (2.22) are characterized by the same order of approximation and the stability condition, as those derived from (2.17) – (2.19) by modifications of the grid area.

2.1.2. The transition to the complex amplitude

By studying the propagation of monochromatic light through diffractive optical elements, the researcher usually expects the simulation results in the form of the complex amplitude of the electric field. Strictly speaking, the computational experiment does not generate a monochromatic wave, since prior to the experiment radiation may be absent in the field, but at the selected time T the field in the relevant region can be accurately considered as monochromatic. In computational practice there are several ways of transition from the time domain to the frequency domain in implementing the difference method for the solution of Maxwell's equations.

In [9], one of the first on the issue, the intensity of the resultant electric field was determined by the addition of the intensities at different layers of the grid area in the time chosen for a certain period, followed by averaging. The specified method is similar to the principle of integral intensity sensors used in the formulation of field optical experiments, and is characterized by simplicity of implementation. However, this approach can not provide information about the phase of the complex electric field amplitude and is associated with a large number of additional arithmetic operations. The researcher needs to define the averaging of the intensities in the time interval equal to at least one period of oscillation of the electric field in the steady mode.

The use of Fourier transforms to switch to the frequency domain [23] provides information not only on the modulus of the complex amplitude of the electric field, but also the phase. It is necessary to consider the value of the grid function of strength for all time sections relating to the period of oscillations of the field in the steady mode. Thus, the second way of transition to the frequency domain also requires large computational costs, differing from the first one by the necessity of applying a Fourier transform.This feature is a major obstacle to constructing the effective vector and parallel procedures for implementing the finite difference solution because of the difficulties in vectorization and parallelization of the fast Fourier transform.

The idea of a third way of transition to the frequency domain has been known for a long time [24], but it has not been implemented as an algorithm in the literature, available to the authors. This is implemented in this monograph.

Following [24, 25], we represent the field in the form of the complex amplitude $\dot{E}_x = \dot{E}_{x_{re}} + i\dot{E}_{x_{im}}$, assuming

$$E_x = \mathrm{Re}\ \left\{\dot{E}_x \exp(-i\omega t)\right\}, \tag{2.32}$$

where ω is cyclic frequency. Then

$$\mathrm{E_x} = \dot{E}_{x_{re}} \mathrm{Cos}\omega\mathrm{t} + \dot{E}_{x_{im}} \mathrm{Sin}\omega\mathrm{t}.$$

The intensity of the field can be determined by means of two measurements of E_x at different times, by solving the equation:

CORRECT

$$\mathrm{E_{x1}} = \dot{E}_{x_{re}} \mathrm{Cos}\omega\mathrm{t}_1 + \dot{E}_{x_{im}} \mathrm{Sin}\omega\mathrm{t}_1, \tag{2.33}$$

$$\mathrm{E_{x2}} = \dot{E}_{x_{re}} \mathrm{Cos}\omega\mathrm{t}_2 + \dot{E}_{x_{im}} \mathrm{Sin}\omega\mathrm{t}_2. \tag{2.34}$$

We agree to take t_1 and $t_2 = T$ such that

$$\omega t_2 = \omega t_1 + \pi / 2.$$

Given that here cos ωt_1 = sin ωt_2, and sin ωt_1 = – cos ωt_2, instead of (2.33) and (2.34) we get

$$\mathrm{E_{x1}} = \dot{E}_{x_{re}} \mathrm{Sin}\omega\mathrm{t}_2 - \dot{E}_{x_{im}} \mathrm{Cos}\omega\mathrm{t}_2,$$

$$\mathrm{E_{x2}} = \dot{E}_{x_{re}} \mathrm{Cos}\omega\mathrm{t}_2 + \dot{E}_{x_{im}} \mathrm{Sin}\omega\mathrm{t}_2.$$

Squaring the last two equations, we add them together:

$$\left(E_{x1}\right)^2 + \left(E_{x2}\right)^2 = \left(\dot{E}_{x_{re}}\right)^2 + \left(\dot{E}_{x_{im}}\right)^2 = \mathrm{I},$$

where I is the unknown quantity which is proportional to light intensity.

For a monochromatic wave, the origin from which t_2 is plotted can be chosen arbitrarily. It is convenient to take $\omega t_2 = \pi / 2 + 2\pi l$, where $l \in N_0$ at which cos $\omega t_2 = 0$, sin $\omega t_2 = 1$. Then

$$\dot{E}_{x_{re}} = \mathrm{E_{x1}},\ \dot{E}_{x_{im}} = \mathrm{E_{x2}}.$$

The foregoing describes the transition in the frequency domain, from E_x to I, which can restrict the choice of two time layers Ex_1 and Ex_2, not using the FFT in the last layers of time, with further averaging the result. This approach significantly simplifies the implementation of the algorithm and reduces the duration of the calculations on it.

The development of the proposed method of transition [26] associated with the replacement (2.32) by

$$E_x = \mathrm{Re}\left\{\dot{E}_x \exp(-i(\omega t - \pi / 2))\right\}, \tag{2.35}$$

that allows the use of (2.35) for the job of the incident wave, matching a job with the most common form of initial conditions – the lack of fields in D before the computer simulation. Indeed, putting (2.35) $t = 0$. we obtain $E_x = 0$ for $\dot{E}_x = 1$. Instead of (2.33) (2.34) we write

$$\mathrm{E_x(t_1)} = \dot{E}_{x_{re}} \mathrm{Sin}\omega\mathrm{t}_1 - \dot{E}_{x_{im}} \mathrm{Cos}\omega\mathrm{t}_1, \tag{2.36}$$

CORRECT

$$\mathrm{E_x(t_2)} = \dot{E}_{x_{re}} \mathrm{Sin}\omega\mathrm{t}_2 - \dot{E}_{x_{im}} \mathrm{Cos}\omega\mathrm{t}_2. \tag{2.37}$$

Assume further t_1 and $t_2 = T$ such that $\omega t_2 = \omega t_1 + \pi / 2$. Substituting this expression into (2.36) (2.37) we get:

$$\mathrm{E_x(t_1)} = -\dot{E}_{x_{re}} \mathrm{Cos\omega T} - \dot{E}_{x_{im}} \mathrm{Sin\omega T},$$

$$\mathrm{E_x(t_2)} = \dot{E}_{x_{re}} \mathrm{Sin\omega T} - \dot{E}_{x_{im}} \mathrm{Cos\omega T}.$$

Solving this system with respect to $\dot{E}_x$, we find:

$$\dot{E}_{x_{re}} = \mathrm{E_x(t_2)Sin\omega T} - \mathrm{E_x(t_1)Cos\omega T},$$

$$\dot{E}_{x_{re}} = -\mathrm{E_x(t_1)Sin\omega T} - \mathrm{E_x(t_2)Cos\omega T}.$$

In contrast to the method described in [25], this approach allows to take into account the phase of the complex amplitude of the incident wave, if such a wave is determined by the representation (2.35). Such consideration is especially important in decomposing the computational domain, impossible in variants of the transition to the frequency domain.

2.1.3. Application of absorbing layers

The task of limiting the computational domain has an important place in difference solutions of Maxwells' equations. In most cases, the researcher must submit either an optical element, surrounded by a homogeneous medium (e.g. free space), or located at the interface between two semi-infinite media. This is connected with the general tendency of physics to reductionism, when it is attempted to distinguish the phenomena from the surrounding world and consider them separately from external influences. This approach seems most appropriate in the majority of cases.

The researcher is forced to image the computational domain as an infinite homogeneous space extending in any given direction, or as the interface between two such spaces. Otherwise, the processes occurring behind the region have an impact on the processes inside. For example, the wave leaving the region is reflected from an external object and comes back.

However, carrying out simulation for computer engineering, characterized by a given speed, the selected area of memory, and having a limited supply of time, the researcher can not solve the difference problem in infinite space.

Fortunately, this is not required if the area of interest (in which the field distribution is taken as the solution of the problem) is finite, and the processes in this region occur at a given time interval.

In this case it is sufficient to trace the distribution of the scattered field in a homogeneous infinite space outside the region of interest only in places where it has time to spread during the experiment.

Clearly the desire of the researcher is not to study the fate of the radiation leaving the vicinity of the optical element being studied. Is it possible to impose the boundary conditions or carry out the appropriate structuring of the subregion adjacent to the border, allowing outgoing radiation *D* not to come back?

None of the above boundary conditions provides such an effect. Moreover, none of these conditions allow the scattered radiation to leave the experiment region, which leads to the inevitable distortion of the result. Next, we consider approaches to avoid such a distortion.

2.1.3.1. Formulation of absorbing boundary conditions and the imposition of absorbing layers

The first effective approach to solving the problem [27] is based on the factorization of the wave operator. In the two-dimensional case, writing the d'Alembert operator in the form

$$G \equiv \frac{\partial^2}{\partial x^2} + \frac{\partial^2}{\partial z^2} - \frac{1}{c^2}\frac{\partial^2}{\partial t^2} \equiv D_x^2 + D_z^2 - \frac{1}{c^2}D_t^2,$$

looking for his performance as

$$G \equiv G^+ G^-,$$

where

$$G^+ \equiv D_z + \frac{D_t}{c}\sqrt{1 - S^2}$$

corresponds to the wave propagation inside the two-dimensional computational domain from the left border, and

$$G^- \equiv D_z - \frac{D_t}{c}\sqrt{1 - S^2}. \tag{2.38}$$

corresponds to the propagation outside the region. At the same time $S \equiv \frac{D_y}{D_t / c}$.

The authors of [27] have shown that the solution at the selected boundary of the equation $G^- U = 0$, where function U characterizes the electromagnetic field equivalent to the boundary condition, which is absorbing the waves and tends to leave D through the left border. At the same time, all plane waves incident on the boundary at any angle are absorbed. For the right edge of the computational domain the absorbing condition is the equation $G^+ U = 0$. Similarly, we seek a factorization of the d'Alembert operator in the formulation of the absorbing conditions at the upper and lower boundaries.

Practical implementation of the approach is associated with the decomposition of the radical from (2.38) into a series. For example, taking

$$\sqrt{1 - S^2} \cong 1 - \frac{1}{2}S^2. \tag{2.39}$$

we write

$$G^- \cong D_z - \frac{D_t}{c} + \frac{cD_y^2}{2D_t}.$$

Then, the absorbing boundary conditions take the form:

$$\frac{\partial^2 U}{\partial z \partial t} - \frac{1}{c}\frac{\partial^2 U}{\partial t^2} + \frac{c}{2}\frac{\partial^2 U}{\partial y^2} = 0 \text{ on the left boundary,} \tag{2.40}$$

$$\frac{\partial^2 U}{\partial z \partial t} + \frac{1}{c}\frac{\partial^2 U}{\partial t^2} - \frac{c}{2}\frac{\partial^2 U}{\partial y^2} = 0 \text{ on the right boundary,} \tag{2.41}$$

$$\frac{\partial^2 U}{\partial y \partial t} - \frac{1}{c}\frac{\partial^2 U}{\partial t^2} + \frac{c}{2}\frac{\partial^2 U}{\partial z^2} = 0 \text{ at the upper boundary,} \tag{2.42}$$

$$\frac{\partial^2 U}{\partial y \partial t} + \frac{1}{c}\frac{\partial^2 U}{\partial t^2} - \frac{c}{2}\frac{\partial^2 U}{\partial z^2} = 0 \text{ at the lower boundary.} \tag{2.43}$$

The Difference approximation (2.40)–(2.43) for the solution of Maxwell‘s equations associated with the name Mur [28], and the absorbing boundary conditions are also often referred to as the Mur and the whole approach as a whole.

The ‘bottleneck’ of the method is the decomposition (2.39) which has been repeatedly improved [29.7] and still remains a source of error.

A better approach does not involve formulation of the boundary conditions other than those listed in section 2.1.1. The absorption of the field leaving the computational domain is achieved by arranging a specific evironment at the borders Γ which does not transmit electromagnetic radiation and does not reflect it.

One of the methods of constructing such an environment is associated with the representation of Maxwell’s equations in the form of [8.30]:

$$\text{rot } \mathbf{H} = \frac{\partial \mathbf{D}}{\partial t} + \mathbf{j},\ \text{rot } \mathbf{E} = -\frac{\partial \mathbf{B}}{\partial t} - \mathbf{j}^*, \tag{2.44}$$

where j^* is the density of magnetic current, which is equal to $\sigma^* H$, σ^* is the magnetic conductivity of the medium. Subject to the conditions

$$\sigma / \varepsilon_0 = \sigma^* / \mu_0 \tag{2.45}$$

the wave impedance in such an environment for $\varepsilon = \mu = 1$ is the wave impedance in vacuum, therefore, there is no reflection from the absorbing layer (in the incidence on it of a plane wave at an arbitrary angle) [7]. In the layer the wave energy spill over into the energy of currents and the field is damped.

In the one-dimensional case, the equations (2.44) can be written as

$$\varepsilon_0 \varepsilon \frac{\partial E_x}{\partial t} + \sigma E_x = -\frac{\partial H_y}{\partial z},\ \mu_0 \frac{\partial H_y}{\partial t} + \sigma^* H_y = -\frac{\partial E_x}{\partial z}. \tag{2.46}$$

The two-dimensional version looks like:

$$\mu_0 \frac{\partial H_y}{\partial t} + \sigma^* H_y = -\frac{\partial E_x}{\partial z},\ \mu_0 \frac{\partial H_z}{\partial t} + \sigma^* H_z = \frac{\partial E_x}{\partial y},$$

$$\varepsilon_0 \varepsilon \frac{\partial E_x}{\partial t} + \sigma E_x = \frac{\partial H_z}{\partial y} - \frac{\partial H_y}{\partial z}.$$

Introducing the propagation and attenuation of the field along different directions by separate equations leads to the splitting of the electric component and conductivities, recording [8,7]:

$$\mu_0 \frac{\partial H_y}{\partial t} + \sigma_z^* H_y = -\frac{\partial \left(E_{xy} + E_{xz} \right)}{\partial z}, \tag{2.47}$$

and

$$\frac{\partial H_z}{\partial t} + \sigma_y^* H_z = \frac{\partial \left(E_{xy} + E_{xz} \right)}{\partial y}, \tag{2.48}$$

$$\varepsilon_0 \varepsilon \frac{\partial E_{xy}}{\partial t} + \sigma_y E_{xy} = \frac{\partial H_z}{\partial y}, \tag{2.49}$$

$$\frac{\partial E_{xz}}{\partial t} + \sigma_z E_{xz} = -\frac{\partial H_y}{\partial z}, \tag{2.50}$$

where $E_x = E_{xy} + E_{xz}$, and condition (2.45) should be observed for the corresponding projections of the conductivities.

Then the attenuation in the direction Z will provide the non-zero conductivity, σ_z^*, σ_z in the solution of (2.47), (2.50). In the direction of $Y - \sigma_z^*, \sigma_y$, in the solution of (2.48), (2.49).

The location of the absorbing layers in the one case (Fig. 2.9) corresponds to the placement of the domain in the shell.

In computational practice [8,7] the conductivities are defined by determining their value in the absorbing layers using the rule

$$\sigma = \sigma_{\max} \left(\frac{L - L_z + z}{L} \right)^q \text{ To the right of the layer } (L_z - L \le z \le L_z),$$

$$\sigma = \sigma_{\max} \left(\frac{L - z}{L} \right)^q \text{ To the left of the layer } (0 \le z \le L),$$

where $q \in R$. Thus, the conductivity of the layer increases towards the boundary and reaches its maximum value there. The magnetic conductivity σ^* is defined in terms of σ (2.45).

The two-dimensional case corresponds to the location of the absorbing layers, shown in Fig. 2.10 [8.7].

In subareas 2 and 6 (Fig. 2.10) there are non–zero components σ_y and σ_y^*. In subareas 4 and 8 components σ_z and σ_z^*, in 1, 3, 5, 7 both projections σ and σ^* different from zero (provided the attenuation of a wave propagating in any direction).

Then

$$\sigma_y = \sigma_{\max} \left(\frac{L - y}{L} \right)^q, \text{ at } 0 \le y \le L \text{ in subregions 1, 2, 3;}$$

$$\sigma_y = \sigma_{\max} \left(\frac{L - L_y + y}{L} \right)^q, \text{ at } Ly–L \le y \le Ly \text{ in subregions 5, 6, 7;}$$

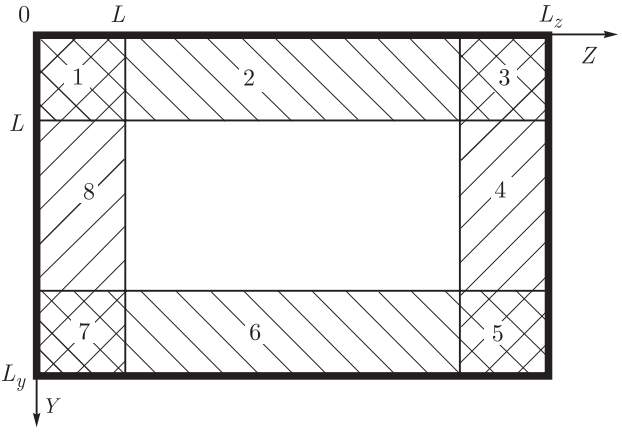

Fig. 2.10. Position of absorbing lauers in the two-dimensional case. The layers are crosshatched, L_z is the length of the computational domain in direction Z; L_y is the length of the computational domain in direction Y; L is the thickness of the absorbing layers.

$$\sigma_z = \sigma_{\max}\left(\frac{L-z}{L}\right)^q, \text{ at } 0 \le z \le L \text{ in subregions 1, 8, 7;}$$

$$\sigma_z = \sigma_{\max}\left(\frac{L-L_z+z}{L}\right)^q, \text{ at } L_z - L \le z \le L_z \text{ in subregions 3, 4, 5.}$$

Any projection of the magnetic conductivity is determined by the corresponding projection of the electrical conductivity of (2.45).

2.1.3.2. The difference approximation of Maxwell's equations in absorbing layers

The location of the absorbing layers at the borders of the computational domain allows any boundary conditions to be set. It is traditionally accepted [8,7] to set the electric wall.

Then in the one-dimensional solution (2.46) on D_h^1 we write the Yee explicit difference scheme in the absorption region:

$$\begin{aligned}
&\mu_0 \frac{H_{y_{k+0.5}}^{m+0.5} - H_{y_{k+0.5}}^{m-0.5}}{h_t} + \sigma_{k+0.5}^{*} H_{y_{k+0.5}}^{m-0.5} = -\frac{E_{x_{k+1}}^{m} - E_{x_k}^{m}}{h_z};\\
&\varepsilon_0 \varepsilon_k \frac{E_{x_k}^{m+1} - E_{x_k}^{m}}{h_t} + \sigma_k E_{x_k}^{m} = -\frac{H_{y_{k+0.5}}^{m+0.5} - H_{y_{k-0.5}}^{m+0.5}}{h_z},
\end{aligned} \tag{2.51}$$

where the subscripts $1 \le k \le L / h_z$ correspond to left absorbing layer for the electric field and $0 \le k \le L/h_z - 1$ for magnetic, and $K - L / h_z \le k \le K - 1$ to the right layer for the electric field and $K - L / h_z \le k \le K-1$ for the magnetic field (Fig. 2.9).

In the two-dimensional solution for (2.47)–(2.5) on D_h^1 we wrire the Yee explicit difference scheme in the absorption region:

$$\mu_0 \frac{H_{y_{j,k+0.5}}^{m+0.5} - H_{y_{j,k+0.5}}^{m-0.5}}{h_t} + \sigma_{z_{j,k+0.5}}^* H_{y_{j,k+0.5}}^{m-0.5} = -\frac{E_{xy_{j,k+1}}^m + E_{xz_{j,k+1}}^m - E_{xy_{j,k}}^m - E_{xz_{j,k}}^m}{h_z};$$

$$\mu_0 \frac{H_{z_{j+0.5,k}}^{m+0.5} - H_{z_{j+0.5,k}}^{m-0.5}}{h_t} + \sigma_{z_{j+0.5,k}}^* H_{z_{j+0.5,k}}^{m-0.5} = \frac{E_{xy_{j+1,k}}^m + E_{xy_{j+1,k}}^m - E_{xz_{j,k}}^m - E_{xz_{j,k}}^m}{h_y};$$

$$\varepsilon_0 \varepsilon_{j,k} \frac{E_{xy_{j,k}}^{m+1} - E_{xy_{j,k}}^m}{h_t} + \sigma_{y_{j,k}} E_{xy_{j,k}}^m = \frac{H_{z_{j+0.5,k}}^{m+0.5} - H_{z_{j-0.5,k}}^{m+0.5}}{h_y}; \tag{2.52}$$

$$\varepsilon_0 \varepsilon_{j,k} \frac{E_{xz_{j,k}}^{m+1} - E_{xz_{j,k}}^m}{h_t} + \sigma_{z_{j,k}} E_{xz_{j,k}}^m = -\frac{H_{y_{j,k+0.5}}^{m+0.5} - H_{y_{j,k-0.5}}^{m+0.5}}{h_z}.$$

We restrict the grid subdomain 1 (Fig. 2.10) the indices $1 \le j \le L / h_y$ and $1 \le k \leqslant L / h_z$ – for E_x (both components of the cleavage), $1 \leqslant j \le L / h_y$ and $0 \le k \le L/h_z - 1$ – to H_y, $0 \le j \le L / h_y - 1$ and $1 \le k \le L / h_z$ – for H_z; subdomain 2 indices $1 \le j \le L / h_y$ and $L / h_z + 1 \le k \le K - L/h_z - 1$ – For E_x, $1 \le j \le L / h_y$ and $L / h_z \le k \le K - L/h_z - 1$ – for H_y, $0 \le j \le L/h_y - 1$ and $L / h_z + 1 \le k \le K - L/h_z - 1$ – for H_z; subdomain three indices $1 \le j \le L / h_y$ and $K - L / h_z \le k \le K - 1$ – for the E_x, $1 \le j \le L / h_y$ and $K - L / h_z \le k \le K - 1$ – for H_y, $0 \le j \le L/h_y - 1$ and $K - L / h_z \le k \le K - 1$ – for H_z; subdomain four indices $L / h_y + 1 \le j \le J - L/h_y - 1$ and $K - L / h_z \le k \le K - 1$ – for E_x, $L / h_y + 1 \le j \le J - L/h_y - 1$ and $K - L / h_z \le k \le K - 1$ – for h_y, $L / h_y \le j \le J - L/h_y - 1$, $K - L / h_z \le k \le K - 1$ – for H_z; 5 subdomain indexes $J - L / h_y \le j \le J - 1$ and $K - L / h_z \le k \le K - 1$ – for the E_x, $J - L / h_y \le j \le J - 1$ and $K - L / h_z \le k \le K - 1$ – for H_y, $J - L / h_y \le j \le J - 1$, $K - L / h_z \le k \le K - 1$ – for H_z; subdomain six indices $J - L / h_y \le j \le J - 1$ and $L / h_z + 1 \le k \le K - L / h_z - 1$ – for E_x, $J - L / h_y \le j \le J - 1$ and $L / h_z \le k \le K - L/h_z - 1$ – for H_y, $J - L / h_y \le j \le J - 1$ and $L / h_z + 1 \le k \le K - L / h_z - 1$ – for H_z; subdomain index 7 $J - L / h_y \le j \le J - 1$ and $1 \le k \le L / h_z$ – for E_x, $J - L / h_y \le j \le J - 1$'s and $0 \le k \le L/h_z - 1$ – to H_y, $J - L / h_y \le j \le J - 1$ and $1 \le k \le L / h_z$ – for H_z; subdomain index 8 $L / h_y + 1 \le j \le J - L/h_y - 1$ and $1 \le k \le L / h_z$ – For E_x, $L / h_y + 1 \le j \le J - L/h_y - 1$ and $0 \le k \le L/h_z - 1$ – for H_y, $L / h_y \le j \le J - L/h_y - 1$ and $1 \le k \le L / h_z$ – for H_z. Then the grid subdomain without absorption located in the range of $L / h_y + 1 \le j \le J - L/h_y - 1$ and $L / h_z + 1 \le k \le K - L/h_z - 1$ for E_x, $L / h_y + 1 \le j \le J - L/h_y - 1$ and $L / h_z \le k \le K - L/h_z - 1$ – for H_y, $L / h_y \le j \le J - L/h_y - 1$ and $L / h_z + 1 \le k \le K - L/h_z - 1$ – for H_z. The thickness of the absorbing layers L is selected in multiple steps of discretization (so that the results of all divisions are integers).

2.1.3.3. Association of absorbing layers in vectorization of calculations

The vector algorithms discussed in 2.1, will also be used in the solution (2.51), (2.52) with the following additions.

In the one-dimensional case, the algorithm for solving Maxwell's equations operated with the vector of the grid function of the strength of the electric field of length K–1 and the vector of the grid function of the magnetic field strength of length K. The imposition of absorbing layers reduces the length of the vectors, and their numbers increases due to the need for separate solutions of equations (2.46) in the absorbing layers and (2.1), (2.2) in the subregion without being absorbed. Namely, putting $w = L / h_z$ for the number of nodes in the grid region, coinciding with the absorbing layers, we will continue to operate with two vectors of length w and a single vector of length of K–1–2w in the calculation of the electric field and the two vectors of length w and a single vecto of length K–2w in calculation of the magnetic field.

Reducing the length of vectors as a rule leads to an increase in the duration of the calculations [19.20] (even at a fixed computational complexity of the algorithm), and complicates writing and adjusting the programs.

In an effort to preserve the old length of the vectors, we can write equation (2.46), not only in absorbing layers, but on the whole grid area D_h^1, using in a non-absorbing medium values of the conductivity equal to zero. However, this method is characterized by the need to allocate additional memory to store the input values of the conductivities (even though they are equal to zero), and by an increase in the number of arithmetic operations (even if these are operations with zeros).

Another approach [18], although it does not not reduce the number of vectors to one for each component of the field, it can reduce it from three to two.

We write the cyclic boundary condition for for the computational domain instead of setting an electric wall, and solve the equation (2.51) for $\tilde{D}_h^1$ instead of $D^1_{h.}$

This technique can be used due to the property of absorbing layers not to transmit the electromagnetic radiation. Radiation does not propagate to the edges of the field, therefore, for the calculation accuracy it is not important which of the three boundary conditions is located there.

In addition, this change allows us to look at the computational domain somewhat differently: for the point $z = 0$ we can choose any node $\tilde{D}_h^1$, since the circular area has no edges. Shifting the origin on L to the right (Fig. 2.9) we come to the area in Fig. 2.11, which also corresponds to $\tilde{D}_h^1$.

As a result, two absorbing layers of length L are merged into one layer with length 2L, for which

$$\sigma = \sigma_{\max}\left(\frac{2L - L_z + z}{L}\right)^q \quad \text{To the left side of the layer } (L_z - 2L \le z \le L_z - L);$$

$$\sigma = \sigma_{\max}\left(\frac{L_z - z}{L}\right)^q \quad \text{To the right side of the layer } (L_z - L \le z \le Lz).$$

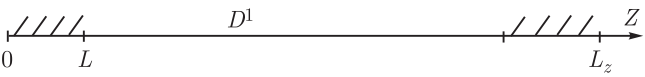

Fig. 2.11. The location of the absorbing layers in the one-dimensional case in the formulation of the cyclic boundary conditions and shift of the origin on the coordinates, 2L is the thickness of the combined absorbing layers.

Then, in the solution of (2.1), (2.2) in the non–absorbing subregion and (2.46) in the combined absorbing layer, we will operate with two vectors of the grid function of the strength of the electric field of length K–1–2w, 2w, and two vectors of the grid function of magnetic field strength of length K –2w, 2w.

Turning to the two-dimensional case, we note that after the imposition of absorbing layers, the electric field vector and both components of the magnetic field split into three subvectors, regardless of the method of storage: a row- or column-orinted. In the row-oriented method decomposition is performed along the direction Z, in column one – along Y.

Unlike the one-dimensional case the increase in the allocated memory when organizing the calculations will be associated not only with the need to store the values of conductivity (which in the scheme (2.17) – (2.19) was not the case), but also with the placement in the memory the electric field split into two components (in absorbing layers). Therefore, leaving the old length of the vectors we have to place in the memory permeability values and split the components of the electric field in a non-absorbing subregion.

In search of a compromise variant, we can write (2.52) in $\tilde{D}_h^2$ in place of D_h^2 [18], replacing the electric wall at the boundary by the cyclic conditions. In the one-dimensional case, such a change corresponds to the transition from a segment to a ring, in the two-dimensional case from a rectangle to a torus.

Shifting the origin on L down and to the right (Fig. 2.10) we come to the area in Fig. 2.12, which also corresponds to $\tilde{D}_h^2$.

In layer A (Fig. 2.12) the layers 8 and 4 merge (Fig. 2.10); in layer B the layers 1, 3, 5, 7 merge, and in C – 2, 6. The following equalities hold for the projection of the electrical conductivity on the Y-axis:

$$\sigma_y = \sigma_{\max}\left(\frac{2L - L_y + y}{L}\right)^q \text{ at the top of the layers C, B } (L_y - 2L \le y \le L_y - L);$$

$$\sigma_y = \sigma_{\max}\left(\frac{L_y - y}{L}\right)^q \text{ at the bottom of the layers, C, B } (L_y - L \le y \le L_y).$$

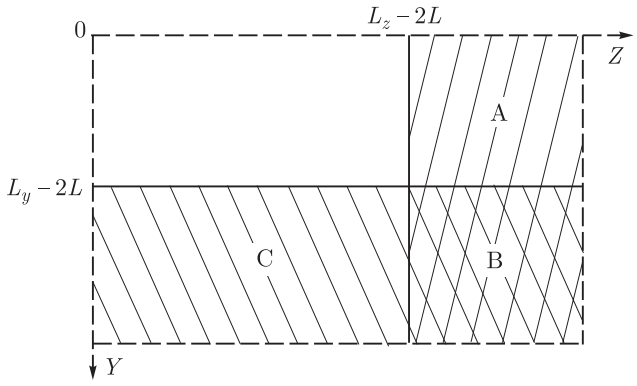

Fig. 2.12. Location of absorbing layers in the two-dimensional case in the formulation of cyclic boundary conditions and the shift of the origin, 2L – combined thickness of the absorbing layers.

The projection of the electrical conductivity on *Z* satisfies the expression:

$$\sigma_z = \sigma_{\max}\left(\frac{2L - L_z + z}{L}\right)^q \text{ the left side of the layers A, B } (L_z - 2L \le z \le L_z - L);$$

$$\sigma_z = \sigma_{\max}\left(\frac{L_z - z}{L}\right)^q \text{ the right side of the layers A, B } (L_z - L \le z \le L_z).$$

Then, in the solution of (2.18) – (2.19) in a non-absorbing subregion and (2.52) in the absorbing layers, we will operate with the two vectors when setting the values of network functions of the two projections of the magnetic field. The electric field in a non-absorbing subregion is specified by one vector and two vectors of the split components in the absorbing layers.

The proposed layout of the absorbing layers in the network domains $\tilde{D}_h^1$ and $\tilde{D}_h^2$ can not only shorten the calculations, but also greatly simplify the writing and debugging the code. Earlier in the simulation of diffraction in the two[-dimensional region it was necessary to finite difference equations in eight absorbing layers and one non-absorbing subregion, also to match the solutions at all 12 boundaries of the layers and subregions.

For example, during the transition from layer 8 (Fig. 2.10) to the central subregion in the direction *Z* the grid projection of the magnetic field on the *Y*-axis does not require the determination by the formulas (2.52) for the absorbing layer and not by (2.17)–(2.19) for the non-absorbing subregion, and needs to write a difference equation that contains the electric field of the central subregion and split components from layer 8:

$$\mu_0 \frac{H_{y_{j,k+0.5}}^{m+0.5} - H_{y_{j,k+0.5}}^{m-0.5}}{h_t} = -\frac{E_{x_{j,k+1}}^m - E_{xy_{j,k}}^m - E_{xz_{j,k}}^m}{h_z},$$

where $L/h_y+1 \le j \le J - L/h_y - 1$ and $k = L / h_z$.

After the unification of the layers the solution is obtained in three absorbing layers and a non-absorbing subregion with the coordination of the fields at eight boundaries (Fig. 2.12). The number of subregions declined by more than half and that of the the borders by a third; the code, written in Fortran 90 and Matlab, allowing the organization of vector calculations, was approximately halved

2.1.3.4. Universal grid areas

In addition to simplicity, the presented layout areas $\tilde{D}_h^1$ and $\tilde{D}_h^2$ are characterized by high flexibility. The one-dimensional or two–dimensional difference Yee scheme on overlapping rectangular grid areas with any boundary conditions from section 2.1.1 can be reduced to writing equations on $\tilde{D}_h^1$ or $\tilde{D}_h^2$. Confirming this, we consider several examples, most frequently encountered in modelling the diffraction of laser radiation on microoptics elements. In this case, the mentioned grid areas with the merged absorbing layers will be called universal.

Example 1. A bounded cylindrical element

One of the most common cases is the study of a finite cylindrical optical element fully placed in D^2. Assume that the parameters of absorbing layers (values of the conductivities and the value of the exponent q) have been selected previously for a perfectly conducting shell used normally in solving this problem [7]. Indeed, replacement of electric walls (2.20) by the cyclic condition (2.27) – (2.31) will lead to some (albeit small) drop in accuracy.

In practice, reducing the thickness of the absorbing layers, their parameters are selected in such a way that the weakened scattered wave reaches the electric wall, reflects from it and is finally absorbed on the way back through the layer. Replacement of the electrical wall by the cyclic condition leads to a change in the phase of the back propagating wave which does not reflected from a perfect conductor, and comes from the opposite edge of the computational domain (special features of the toroidal structure of the grid area $\tilde{D}_h^2$). The wave with the new phase will be absorbed in the layer, calculated for a different field, to a lesser extent.

If the new selection of parameters of the absorbing layers for achieve the former accuracy is tedious for the researcher, or he prefers to use the standard values, the following small addition to the calculation algorithm is made to improve the situation.

Instead of the boundaries of the region (the cyclic conditions are already defined there), the electric wall is placed in the absorbing layers. To do this, imagine that the transformation to a torus with the union of absorbing layers takes place in region D_h^2 and not $\tilde{D}_h^2$. We merge the electrical walls at the boundaries $z = 0$, $z = L_z$ $(0 \le y \le L_z)$ which gives a cylindrical surface; then we combine the electrical walls at the boundaries $y = 0$, $y = L_z$ $(0 \le z \le L_z)$ which gives a torus; the origin of the coordinates is then shifted by L to the right and down (Fig. 2.12). This gives the universal grid region (Fig. 2.12) with the electrical walls located on the segments $y = L_y - L$, $0 \le z < L$ and $z = L_z - L$, $0 \le y \le L_y$ (Fig. 2.13)

Performing calculations on such a field, it is not necessary to use the electric and magnetic walls as boundary conditions, writing in their vicinity the difference

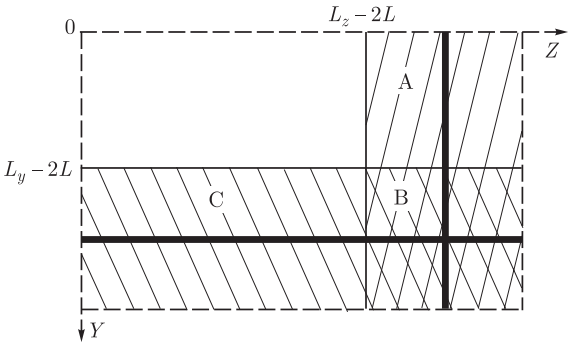

Fig. 2.13. The location of the electrical wall on a universal grid area in the study of an isolated cylindrical optical element. The electric wall is marked by thick bars.

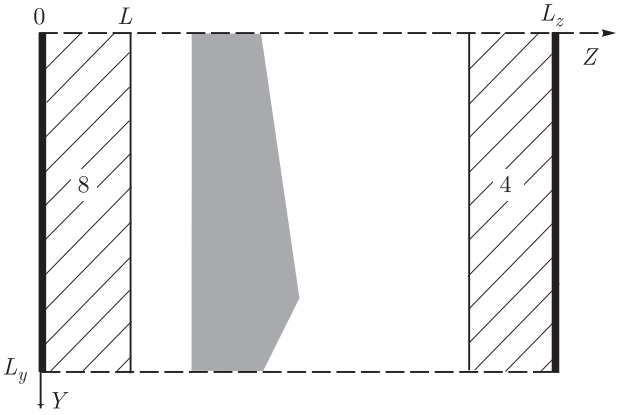

Fig. 2.14. The traditional layout of the computational domain for simulating infinite periodic optical element (a combination of electric walls and cyclic conditions).

equations different from (2.52); this will increase the duration of the calculation, offsetting the gains made at the expense of more successful vectorization.

It is reasonable after the transition to the next temporal layer to reset the values of the network functions of the electric field at the specified intervals. It is enough to multiply the two corresponding vectors by a scalar (elementary vector operation is done in hardware), which is equal to zero. The accuracy of the simulation results on the universal grid area after the proposed modification of the algorithm exactly coincides with the simulation results on D_h^2.

Example 2. An infinite two-dimensional diffraction grating

We assume that the investigated element is periodic along the axis *Y*. It is then sufficient to assumed in the universal grid area that σ_y and σ_y^* are equal to zero to ensure that layer C (Fig. 2.12) does not absorbed the radiation propagating in the directions *Y* and –*Y*, and layer B absorbs only in the directions *Z* and –*Z*. In this case C actually enters into a non-absorbing subarea, the layers A and B can be taken as a single absorbing layer. Similarly, modification of the universal domain in the study of an infinite element, periodic along the axis *Z*, is performed in the same manner

Coordinating solutions on the traditional grid region [23], which combines electric walls at the boundaries $z = 0$, $0 \le y \le L_z$ and $z = L_z$, $0 \le y \le L_y$ with the cyclic boundary conditions at $y = 0$, $0 \le z \le L_z$ and $y = L_y$, $0 \le z \le L_z$ (Fig. 2.14), and the universal grid area, in the combined absorbing layer A we place the electrical wall on the interval $z = L_z - L$, $0 \le y \le L_y$ (Fig. 2.15).

Then the two solutions on these grids coincide.

Example 3. A bounded symmetric cylindrical element

In the study of the propagation of radiation through a bounded symmetrical cylindrical element the magnetic wall is placed on the axis of symmetry. The grid area $\overline{D}_h^2$ encompasses half of the element and in the variant without combining absorbing layers is shown in Fig. 2.16.

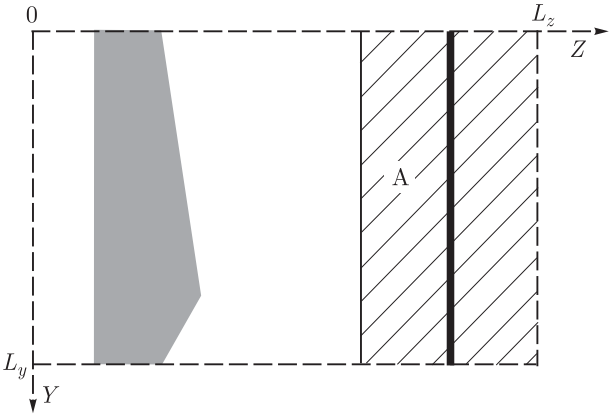

Fig. 2.15. The location of the electrical wall on a universal grid area in the study of an isolated cylindrical optical element.

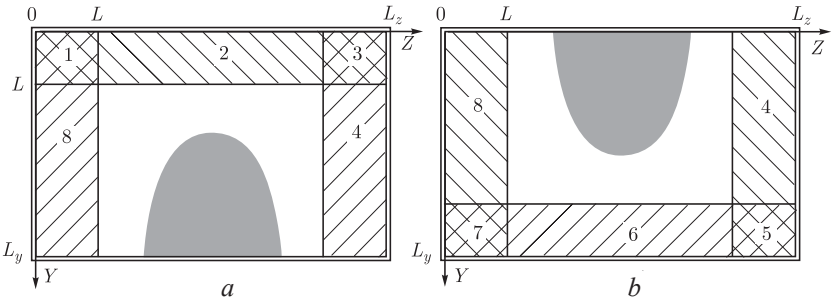

Fig. 2.16. Location of absorbing layers in the field $\bar{D}_h^2$ without their union. Case a) corresponds to the placement into the upper half of the symmetrical elements, case b) – the lower one.

After the combination of layers 4 and 8 (Fig. 2.16) and the transition to $\bar{D}_h^2$, the area of computer simulation will take the form shown in Fig. 2.17.

When the layer 2 in Fig. 2.16a becomes the layer C in Fig. 2.17a, layers 1 and 3 after the merger go to B, sections 4, 8 – to A. Layer 6 in Fig. 2.16b changes to layer C in Fig. 2.17b, layers 5 and 7 after the merger go to B, sections 4, 8 – to A.

Four magnetic walls at the boundaries $\bar{D}_h^2$ change into two walls in the area, located on the segments $y = L$, $0 \le z \le L_z$ and $z = L_z - L$, $0 \le y \le L_y$ (for the case shown in Fig. 2.16a) and at intervals of $y = Ly - L$, $0 \le z \le L_z$ and $z = L_z - L$, $0 \le y \le L_y$ (for the case shown in Fig. 2.17b)

As in *Example 1*, in the universal area one should not regard the magnetic walls as the boundary conditions by writing in their neighborhood new difference equations. It is enough before moving on to the next layer in time to reset the grid components of the vector of projection of the magnetic field projection on the *Z*-axis at $y = L$, $0 \le z \le L_z$ and $z = L_z - L$, $0 \le y \le L_y$ (Fig. 2.17a) or $y = L_y - L$, $0 \le z \le L_z$; also we should reset the grid components of the vector of projection of the magnetic field on the *Y* axis at $z = L_z - L$, $0 \le y \le L_y$ (Fig. 2.17a) or $z = L_z - L$, $0 \le y \le L_y$ (Fig. 2.17b).

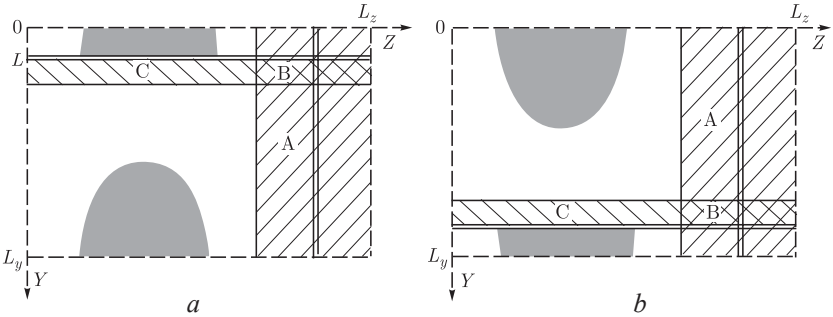

Fig. 2.17. The location of the absorbing layers and magnetic walls (double line) on a universal grid domain in simulation of symmetric elements. Case a) corresponds to the placement in the area in the upper half of the symmetric elements, case b) – the lower one.

It is not compulsory to place the magnetic walls in layers A and B (Fig. 2.17). Surrounded on both sides by an absorbing medium, it will not have a decisive influence on the result of computer simulation. And yet, its absence would cause a slight (usually in the third place for a sufficiently dense mesh) mismatch in the values of field strengths in solution on $\bar{D}_h^2$ and $\tilde{D}_h^2$. The reason for this, as in Example 1, is setting the parameters of an absorbing layer on the interaction of the scattered wave with the magnetic wall. Without this absorption at these parameters will be less effective. One should either install a wall, or pick up new parameters of the layers (absorbing the radiation propagating in the direction of *Z*), to ensure an acceptable accuracy. The latter option requires different settings of the absorption in the *Y*- (where the magnetic wall remains) and *Z*-directions (where the wall is removed).

Example 4. An infinite periodic symmetric element

When considering in Section 2.1 the boundary conditions applied to modelling the propagation of electromagnetic waves through an infinite periodic symmetric element, it was concluded that it is adequate to install the magnetic walls on all boundaries of the computational domain. Taking the axis *Y* as the periodicity direction, the absorbing layers are positioned on $\bar{D}_h^2$ as shown in Fig. 2.18.

The transition to universal net area is associated with the adoption of conductivity σ_y and σ_y^* equal to zero (as in *Example 2*) and the placement of magnetic walls at intervals of $y = L$, $0 \le z \le L_z$ and $z = L_z - L$, $0 \le y \le L_y$. Then the computational domain takes the form shown in Fig. 2.19.

As in the previous examples, it is not necessary to place the magnetic wall in layer A (Fig. 2.19), and the parameters of the absorbing layers can be selected for the case without the wall.

As seen from the four examples, varying the values of vector components of the conductivities σ, σ^* and placing the electric or magnetic walls inside $\tilde{D}_h^2$, the proposed optical elements can be studied using the universal grid area. Moreover, selecting the optimal parameters of the absorbing layers in areas A,

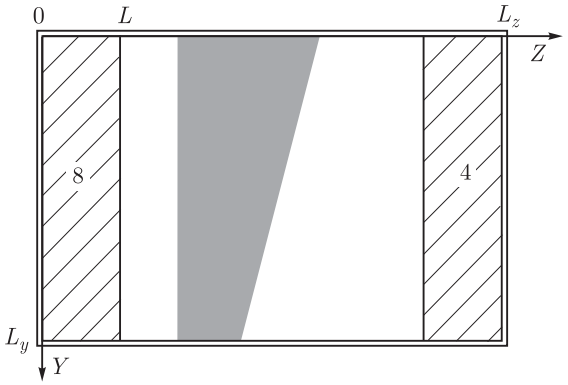

Fig. 2.18. The location of the absorbing layers in the region without combining them in the study of the periodic symmetric element.

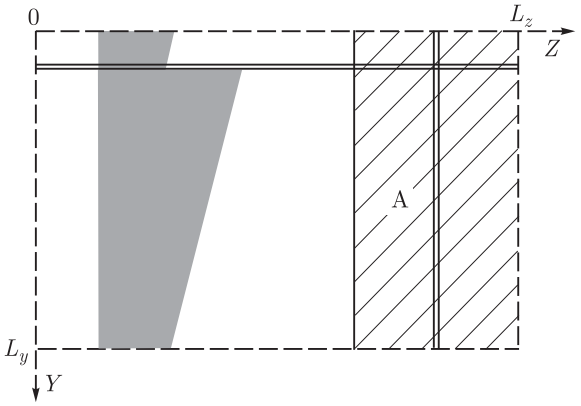

Fig. 2.19. The layout of the universal grid area in the study of the periodic symmetric element.

B, C (Fig. 2.12), the researcher is free not to place the electric wall on $\tilde{D}_h^2$ and place the magnetic walls only when they are not inside the absorbing layers (hor izontal magnetic walls in Figs. 2.16, 2.19). This optimization eliminates the need to reset before switching to a new temporary layer of the corresponding components of the electromagnetic field

2.1.4. Formation of the incident wave

Modelling the propagation of radiation through the optical element, in addition to imposing the grid region and write on it difference equations, it is also necsaary to define the field coming from the outside and incident on the element.

Indeed, the result will depend not only on the geometry of the investigated optical element and the material from which it is made, but also on the type of incident electromagnetic wave – the distribution of complex amplitudes of the projections of its vectors in space and time.

A separate task should be matching of the techniques of setting the incident field, boundary conditions, the method of imposing absorbing layers and topography of the investigated element. Some methods of forming the incident wave are used in the study of elements, working on in transmission and reflection, periodical and non-periodical deposited on a substrate or without it, located in free space or formed at the end of the optical waveguide.

The choice of the method of forming the incident wave will determine the features of the implementation of algorithms for the difference schemes. The type of method determines both the accuracy and duration of computer simulation. Vector and parallel algorithms are written in different ways for different technology tasks of the incident field.

By limiting the scope of the subject area of optics, we exclude from consideration the methods of excitation of the electromagnetic field by the currents, characteristic of electromagnetic problems in general and in particular the theory of antennas [7]. Moreover, we ignore for a time the physical nature of the radiation source and associated methods for defining the field.

Leaving aside the problem of pulse propagation, we will not deal with the problem of their formation and entry into the computational domain, even though all of the following methods can be easily adapted to solve this problem.

In modern literature there are three main approaches to the task of defining the harmonic incident field in the study of diffraction on the optical structures by the finite difference solution of Maxwell‘s equations. Let us examine them in the development, with particular emphasis on modifications applied to the study of microelements, in particular, diffractive optical elements.

2.1.4.1. The method of the‘hard’ source

The first paper on the difference solution of Maxwell equations in differential form, authored by Yee [4], published in 1966, contained a description of the input method of the radiation in the computational domain, later named [7] using ‘the hard source’ method.

The method consists of defining for the selected area of space of the vectors of the electromagnetic field through an analytical representation of the form

$$G(\mathbf{x}_0) = \mathrm{Re}[A(\mathbf{x}_0)\exp(-i\omega t + \phi_0))], \tag{2.53}$$

where $\mathbf{x}_0$ are the coordinates of the point from the selected area; $G(\mathbf{x}_0)$ is the formed value of the selected projection of the strength of the component of the electromagnetic field in x_0 before proceeding to the next the temporary layer; $A(x_0)$ is the given complex amplitude of the incident field for the given projection, the power in the exponent determines the phase of the wave (not the phase of the complex amplitude) with an initial phase ϕ_0. and the cofactor with the exponent defines the harmony of the incident monochromatic field; ω is angular frequency; t is time; Re [..] is the operation of selection of the real part of the expression in square brackets.

In the one–dimensional case, organizing Yee computation schemes, for G it is sufficient to accept to either the electric or magnetic field. Let us consider the first option, defining the 'hard' source at node k of the universal grid area with absorbent layers $\tilde{D}_h^1$ with combined absorbing layers of the difference approximation of expression (2.35):

$$E_{x_k}^m = \mathrm{Re}\left[\exp\left(-i\left(\frac{2\pi h_t c}{\lambda} m - \frac{\pi}{2}\right)\right)\right]. \qquad (2.54)$$

Furthermore, the geometrical dimensions of the computational domain and objects in the domain are measured in wavelengths (unless otherwise specified), putting (2.54) $\lambda = 1$. The parameters of discretization of the grid region are given in the form of pairs of numbers (Q, Q_t). The first number corresponds to the number of nodes in the grid area in space coinciding with the wavelength, the second – the number of nodes over time during which the plane wave front in a vacuum travels a distance of one wavelength.

Organizing the formulation of a computational experiment in free space [18], we take $L_z = 4\lambda$, $L = \lambda$, and the source is located in the leftmost node $\tilde{D}_h^1$ ($k = 0$). During the time $T = 20\ \lambda\ /c$ the field in the studied area is stabilized and can be considered monochromatic.

Choosing in $\tilde{D}_h^1$ discretization (Q, Q_t) = (10, 20), we consider the distribution of the module of the complex amplitude of the electric field in the area of computer simulation (Fig. 2.20).

In the subdomain of arrangement of the absorbing layers ($2 \le z \le 4$) the fieldd decaus, and in free space ($0 \le z \le 2$) a plane homogeneous T-wave propagates. Complete decay to the zero modulus of the complex amplitude in Fig. 2.20 does not occur, since the layers absorbs over its entire length, and the scattered radiation penetrates the layer from both sides.

By studying the dependence of the error of the difference solution on the discretization parameters (Table 2.1), we note the convergence of the difference method for solving Maxwell's equations to the analytical solution for the chosen parameters of the computational experiment.

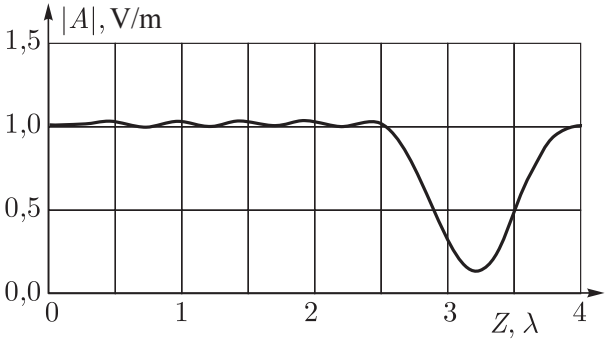

Fig. 2.20. The distribution of the modulus of the complex amplitude of electric field |A| on $\tilde{D}_h^1$ from the 'hard' source.

Table 2.1. Dependence of the errors of numerical experiments for the vacuum on discretization of the grid area (Q, Q_t) and the parameters of absorbing layers σ_{max} and q for the 'hard" source'

(Q,Q_t)	Parameters of absorbing layers		Error values
	σ_{max}, cm/m	Q	ε, %
(10, 20)	0.018	1.5	1,3948
(20, 40)	0.024	2	0.10228
(50, 100)	0.032	2.5	0.03688
(100, 200)	0.037	2.7	0.010405

Table. 2.1 presents the values of the uniform error

$$\varepsilon = \max_k \left| \frac{|B_k| - |A_k|}{|B_k|} \right|, \tag{2.55}$$

where ($1 \le k \le 2Q$), which characterizes the maximum deviation from the analytical solution. In (2.55) value $|B_k|$ is the modulus of the complex amplitude of the electric field in the analytic solution ($|B_k| = 1$ V/m for (2.55)).

In the two-dimensional case, to obtain a homogeneous plane wave in the universal grid region we define a 'hard' a source in the interval $k = 0$; $0 \le j \le J$–1

$$E^m_{x_{j,k}} = \mathrm{Re}\left[\exp\left(-i\left(\frac{2\pi h_t c}{\lambda} m - \frac{\pi}{2} \right) \right) \right]. \tag{2.56}$$

Keeping the settings from the previous experiment, we give a square shape to D_2 ($L_y = L_z$).

The results of numerical experiments coincide with the results for the one-dimensional field, as the wave propagates along the direction Z.

Note that in the D_h^2 region the assignment of a plane homogeneous wave through the 'hard' source is impossible because of the discontinuity of the strength of the electric field at the edges D_h^2.

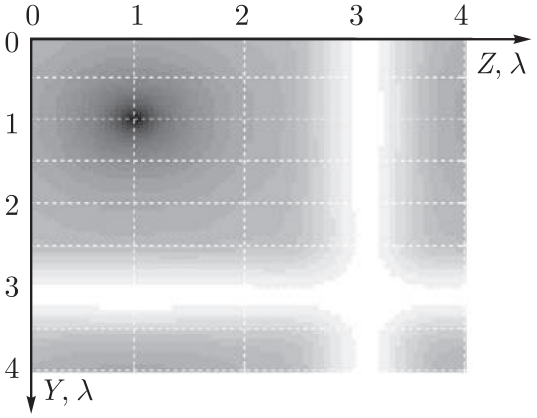

Fig. 2.21. The distribution of the modulus of the complex amplitude of the electric field |A| on $\tilde{D}_h^2$ from a point source.

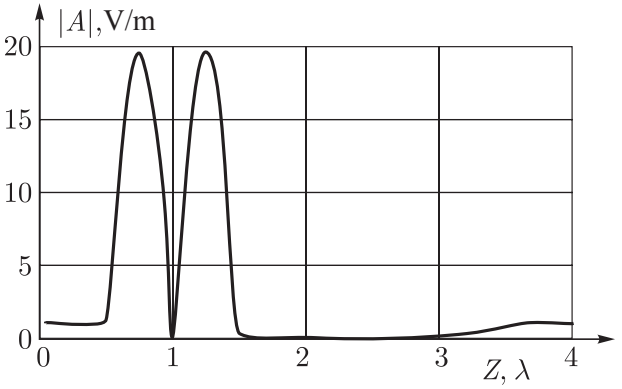

Fig. 2.22. The distribution of the modulus of the complex amplitude of the electric field |A| on $\tilde{D}_h^1$ in wave reflections in between the 'hard' power source and the electric wall.

Figure 2.21 shows the distribution of the field from the point 'hard' source (in (2.56) $j = k = Q$) in free space, defining a cylindrical wave front wave with discretization parameters $(Q, Q_t) = (20, 40)$.

At the locations of the absorbing layer on a universal grid area ($0 \le y \le 2$, $2 \le z \le 4$ – layer A; $2 \le y \le 4$, $2 \le z \le 4$ – layer B and $2 \le y \le 4$, $0 \le z \le 2$ – layer C in Fig. 2.12) the field attenuates.

Characterized by the simplicity of definition and high accuracy, the 'hard' source is of limited use in computational practice. Definition of the incident wave by the equation (2.53) does not allow the wave reflected from the optical object being studied to pass through the 'hard' source and reach the absorbing layer.

Confirming this, we set up a computer experiment, which differs from the previous experiment by the first position of the radiation source (now $k = Q / 2$, $z = 0.5$) and by discretization of the grid area.

Figure 2.22 shows the result of simulation, when installed the electric wall is situated in a node $3Q / 2$ ($z = 1.5$) and reflects the incident wave back toward the source.

Considering the field in the subdomain $0 \le z \le 0.5$, we note the presence of the homogeneous wave radiated in the direction –Z by the 'hard' source that radiates in both directions. The mentioned wave attanueates in the absorbing layer $2 \le z \le 4$ and fades almost completely. Directly behind the electric wall $z = 1.5$ the field is absent. The field reflected from the wall does not pass over the source, and reflecting from it and the wall interferes with the field incident in the direction Z.

Consequently, when using the 'hard' source the source must be sufficiently distant from the area of registration of the resulting field so that the wave reflecting from it does not return to the optical element, distorting the diffraction pattern. Using such a method involves a multiple increase in the computational domain and the duration of the experiment which in some cases makes numerical simulation impossible. The 'hard' source is used to solve the auxiliary problems (testing the model, building a 'transparent' source.)

2.1.4.2. The total field formulation method

Obviously, to account for the waves reflected from the object under study, we must somehow find it. In [9, 31] it is suggested to take over the reflected field at the node location of the source result of the calculation of the difference scheme to specify the incident wave before proceeding with the temporary layer???. Then, adding the reflected field with the incident one, we thus define the resulting field in the location of the source. Calculations by this algorithm can be summarized as follows.

Step 1. Calculation of the field by the difference scheme for the entire region of the layer *m*.

Step 2. Determination of the reflected field as a result of the calculations in step 1 in the location of the source node.

Step 3. The calculation of the resultant field at the node of location of the source by adding the reflected field and the analytically calculated incident field with transition to the next time layer.

Later, in [10] the proposed algorithm was termed the total field formulation method.

Repeating the last experiment with the new source, we obtain the complex amplitude distribution shown in Fig. 2.22.

The wave wave from the electrical wall interferes with the incident wave in the direction *Z* (on $0.5 \le z \le 1.5$), passes through the source and is absorbed on $2 \le z \le 4$ (Fig. 2.23). In the subregion $0 \le z \le 0.5$ we observe the superimposition of the wave emitted by the source in the direction Z and the wave reflected from the electrical wall passing through the source and retreating in the direction Z. In the analytic solution there are no oscillations in the specified interval, and in Fig. 2.23 the oscillations of the complex amplitude for $0 \le z \le 0.5$ are due to an error introduced into the solution by the source.

Studying the accuracy of the method of the resultant field, let us consider a homogeneous plane wave propagation in a free environment by repeating the experiments with the new source for 'hard' power, the results are presented in Table. 2.1.

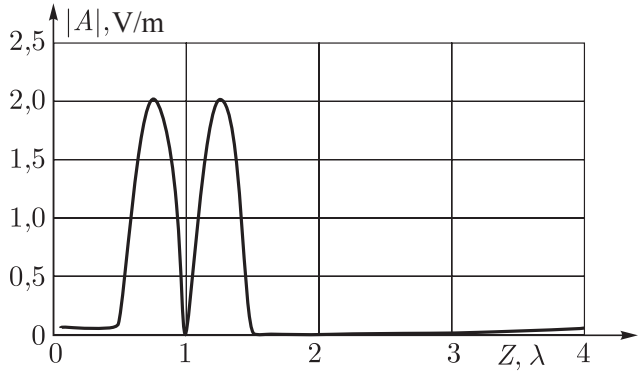

Fig. 2.23. The distribution of the modulus of the complex amplitude of the electric field |A| on $\tilde{D}_h^1$ when using the total field formulation method to specify the incident wave.

Table 2.2. Dependence of the errors of numerical experiments for vacuum on the discretization of the grid area (Q, Q_t) when using the general field method

(Q,Q_t)	(10, 20)	(20, 40)	(50, 100)	(100, 200)
ε, %	8.4609	2.2177	0.37411	0.10187

Comparison of experimental results for free space with the 'hard' source (Table 2.1) and the source given by the total field formulation (see Table 2.2) in not in favour of the latter. The error of results has increased by an order for all discretizations.

The reason for this [18.32] is an error when setting the reflected wave. Developing the method of the general field, it is necessary to determine the reflected wave not as a grid field after the transition to the next time layer, but by setting it by the difference of such a field and a field in another grid areas, devoid of the optical element and therefore free of the reflected wave. Such a source in [18.32] is named 'transparent'.

We formulate the algorithm for defining the 'transparent' source.

Step 1. Field calculation by the difference scheme for the layer m in area with an optical element.

Step 2. Field calculation by the difference scheme for the layer m in the area without the optical element.

Step 3. Determination of the reflected field in the subregion of definition of the source as the difference of the fields between the subdomains found in the first two steps.

Step 4. Setting the resulting wave in the subregion of the source as the sum of analytically given incident field and the reflected field determined in the previous step. Transition a temporary layer m +1.

The calculation results in free space using a 'transparent' source coincided with the data from Table. 2.1: the new source does not introduce any additional error in the difference solution.

By studying the field in the experiment with an electric wall, we see interference extinguishing of the wave in the subdomain $0 \le z \le 0.5$ (Fig. 2.24).

The was reflected from the wall returned to the source in antiphase. Such an exact match with the analytical solutions indicates the absence of the error introduced by the radiation source in the difference solution.

Attention will be given to the formation of the field in the auxiliary problem. It is made in full accordance with 2.1.4.1, when the 'hard' source was used to set a uniform plane wave in free space. In forming the 'transparent' source it is important to choose the grid areas of the auxiliary and main tasks to be fully identical. Differences between the two tasks should be found only in the distribution of the refractive index. The main task has an optical element from which the reflected wave arrives to the source; the auxiliary task does not contain such element and not reflected wave forms in it. If we remove the scatterer also from the main task, the complex amplitude of the reflected wave, determined in setting the 'transparent' source, vanishes by virtue of the identity problems. This accounts for a full match

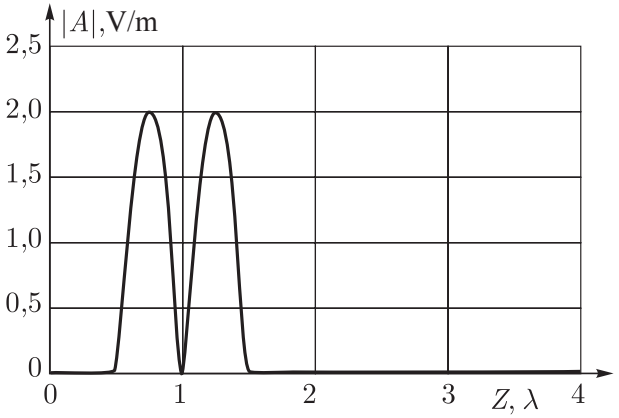

Fig. 2.24. The distribution of the modulus of the complex amplitude of the electric field |A| on $\tilde{D}_h^1$ when using the 'transparent' source to specify the incident wave.

(in all signs) of the calculation results in free space with the use of 'hard' and 'transparent' sources.

In the study of diffractive optical elements the source should be placed in the substrate element (not in vacuum), close to the microrelief in order to reduce the area (in three dimensions – volume) of the computational domain and the duration of the simulation. In this case, the auxiliary problem must contain a homogeneous medium with a refractive index of the substrate, that is the medium of the main task in which the source is located.

The above method of setting 'transparent' source is also true in the case of the two-dimensional computational domain. If in such a field we must set as a uniform a plane wave as an incident wave, it is sufficient for this purpose to process a one-dimensional auxiliary problem, which describes a wave. Only the main task, which contains a two-dimensional optical element, will be two-dimensional

It is important to perform similar calculations on a universal grid area, because for the region with electric walls at the boundaries we can not form a homogeneous plane incident wave through the 'transparent' source. The boundary conditions, given by the electric walls, do not correspond to a uniform plane wave front. For the same reason, it is inappropriate to install the horizontal electric wall in the subareas B and C of the universal grid area (Fig. 2.12). That, however, in no way limits the researcher in choosing the optical elements for modelling, as noted in previous sections. Magnetic walls are compatible with the spread of a homogeneous plane incident wave; hence, symmetric optical elements can be explored through a 'transparent' source.

When specifying other types of incident waves it is necessary to use the two-dimensional auxiliary problem, which is modelled by diffraction of a wave in a homogeneous space through a 'hard' two-dimensional source. An arbitrary incident wave is produced by the appropriate choice of the function of the complex amplitude of the incident wave in (2.53) and by varying the form of the subdomain

of definition of the source (‘hard’ in the auxiliary problem and ‘transparent’ to the main problem).

The method of forming the incident wave from a limited source permits the sharing of the ‘transparent’ source and arbitrarily oriented electric walls at the boundary of the grid area.

2.1.4.3. The method of separation of the field

The idea of defining the incident wave through the separation of the total and scattered (TF/SF) fields was created after [24] the first publication devoted to the total field formulation [31]; it proved to be more productive and popular [7, 33, 34] up to the development of the ‘transparent’ source method [32].

The method consists of limiting the subregion of the resulting field (incident and scattered) by the shell different from the computational domain boundaries and located within such a boundary. The shell is not part of the absorbing layers, located between the layers and the optical element. Behind the shell only the scattered field propagates. The expressions used to separate fields contain terms with the analytically defined incident field; thus, the incident wave is introduced into the subarea of the resulting field. The rest of the subdomain of the computational domain does not contain the incident wave.

A one–dimensional case. For the one-dimensional grid region division is performed in nodes and k_L and k_R (Fig. 2.25 in [7]).

Grid functions at $k_L \le k \le k_R$ refer to the resultant field, the rest – to the scattered one. The difference equations of the Yee scheme Yee [4] in the specified nodes have the form [7]:

$$\varepsilon_0 \varepsilon_{k_L} \frac{E_{x_{k_L}}^{m+1} - E_{x_{k_L}}^{m}}{h_t} = \frac{H_{y_{k_L+0.5}}^{m+0.5} - \left(H_{y_{k_L-0.5}}^{m+0.5} + \tilde{H}_{y_{k_L-0.5}}^{m+0.5} \right)}{h_x}, \tag{2.57}$$

$$\mu_0 \frac{H_{y_{k_L-0.5}}^{m+0.5} - H_{y_{k_L-0.5}}^{m-0.5}}{h_t} = \frac{\left(E_{y_{k_L}}^{m} - \tilde{E}_{y_{k_L}}^{m} \right) - E_{y_{k_L-1}}^{m}}{h_x}, \tag{2.58}$$

$$\varepsilon_0 \varepsilon_{k_R} \frac{E_{x_{k_R}}^{m+1} - E_{x_{k_R}}^{m+1}}{h_t} = \frac{\left(H_{y_{k_R+0.5}}^{m+0.5} + \tilde{H}_{y_{k_R+0.5}}^{m+0.5} \right) - H_{y_{k_R-0.5}}^{m+0.5}}{h_x}, \tag{2.59}$$

$$\mu_0 \frac{H_{y_{k_R+0.5}}^{m+0.5} - H_{y_{k_R+0.5}}^{m-0.5}}{h_t} = \frac{E_{x_{k_R+1}}^{m} - \left(E_{x_{k_R}}^{m} - \tilde{E}_{x_{k_R}}^{m} \right)}{h_x}, \tag{2.60}$$

where the grid functions under the tilde correspond analytically to the given incident field.

The expression (2.57) defines the electrical component in the left node of the resulting field (Fig. 2.25). To do this, we must subtract from each other the strengths of the magnetic field in the neighbouring sites. It is obvious that the subtraction should be carried out for the field strengths of the same nature, in this

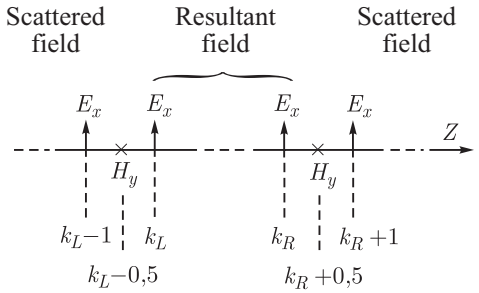

Fig. 2.25. Detail of the one-dimensional grid region [7] with the nodes of of division of resultant and scattered fields.

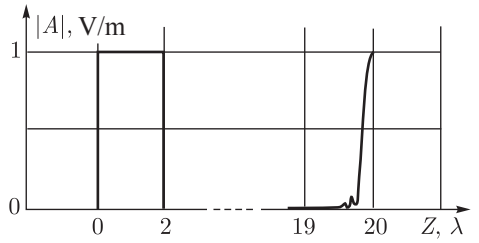

Fig. 2.26. The distribution of the modulus of the complex amplitude of the electric field in the analytic definition of the incident field by the TF/SF method without the imposition of absorbing layers.

case the resultant field strengths, as in (2.57) we calculated precisely the resultant field. But in the difference solution in the node $k_L - 0.5$, only the scattered field is calculated. Therefore, in the right-hand side of (2.57) to the grid function $H^{m+0.5}_{y_{k_L-0.5}}$ we add the value $\tilde{H}^{m+0.5}_{y_{k_L-0.5}}$ of the incident field, which is traditionally given analytically [7].

Similarly, in (2.58) the scattered magnetic field in the node $k_{L-0.5}$ is calculated using the incident electric field $\tilde{E}^m_{y_{k_L}}$ in k_L; the resulting electric field in $k_{R-0.5}$ is calculated from (2.59) through the incident magnetic field in the adjancent right node, and the scattered magnetic field in $k_{R+0.5}$ is determined through the incident electric field $\tilde{E}^m_{x_{k_R}}$ in (2.60).

Further, setting the parameters of numerical experiments, we take $k_L = 1$, $k_R = 2Q$ for the universal one-dimensional grid domain, calculating the error of propagation of a flat homogeneous electromagnetic wave in a vacuum between the two nodes (Table 2.3).

Comparison of the results from Tables 2.1, 2.2 and 2.3 shows that the analytical task of the incident field in the TF/SF method is preferable to the first version of the general field method, but is inferior in accuracy to the variant of the 'transparent' source.

By studying the separated field method, we temporarily abandon the use of absorbing layers, setting the length of the computational domain to 40λ and placing a subdomain of the general field in the middle, leaving the other settings from the

Table 2.3, Dependence on the errors of numerical experiments for vacuum on discretization of the grid area (Q, Q_t) with the formation of the incident wave by the analytical procedure TF/SF in one dimensional case

(Q,Q_t)	(10, 20)	(20, 40)	(50, 100)	(100, 200)
ε, %	2.2289	0.74774	0.20736	0.066696

previous experiment the same. The result of calculations for the discretization (100.200) is shown in Fig. 2.26.

The absence of absorbing layers made it possible [35] to observe the surge of the values of the modulus of complex strength of the electric field at the right end of the grid area (Figure 2.26). This effect is explained by a time delay required for the wave emitted in the node k_L to reach the node k_R. During this delay the wave emitted in k_R propagates in the direction of Z. The waves from these nodes then interfere and mutually cancel each other to the right of k_R. The observed surge leads to the conclusion of non-compliance of the expressions (2.57) – (2.60) with the TF / SF method at the initial stage of the calculation in this case.

The numerical definition of the incident field in (2.57) – (2.60) not only improves the accuracy of calculations [11] and reduces their duration [7] in the two- and three-dimensional cases, but also makes it possible to avoid the above-mentioned effect.

Similar to the procedure used in writing expressions for the 'transparent' source, we consider two problems: the primary and secondary, differing in the methods of defining the incident wave (the 'hard' source for the seconday problem). The values of the electric and magnetic fields found in the secondary problem at the nodes k_L–0.5, k_L, k_R and $k_{L+0.5}$ are substituted into equations (2.57) – (2.60) of the first problem as the incident wave. As noted in [11], this leads to the automatic compensation of numerical errors. The errors in defining the phase shift between the components of the incident field are compensated [35] in the adjacent nodes (k_L–0.5 and k_L; k_R and k_L+0.5), because the analytical definition of the amplitude (2.54) in experiments with a 'hard' source (Table 2.1) is associated with smaller errors.

Indeed, numerical experiments confirm the high accuracy of the difference solution obtained on the basis of the approach proposed in [11]. The resulting error for the selected parameters coincided with the sampling results from Table 2.1. Consequently, the numerical definition of the incident wave in (2.57) – (2.60) did not introduce any additional distortions in the difference solution.

Moreover, because of the disappearance of the time interval between the onset of emission of the wave at the node k_R and the arrival there of waves from k_L, no surges were observed in the right side of the domain (Fig. 2.26).

The above technique is successful when the domain is included in the shell of a homogeneous material. In the simulation of the operation of the diffractive optical element (DOE), this condition is not satisfied. We assume that starting at the node (k_R–k_L) / 2 the left side of the domain is occupied by a homogeneous dielectric half-space (substrate of the DOE) with a refractive index n = 1.5. The error of the transmitted wave will be evaluated on a segment of the boundary between the

Table 2.4. Dependences of the uniform errors of computational experiments for the domain with the insulator (n = 15) / vacuum interface on discretization of the grid area (Q, Q_t) with the formation of the incident wave by various methods TF/SF (a – analytical, b – numerical) in the one–dimensional case.

(Q,Q_t)	Experimental series	
	a	*b*
(10, 20)	7.9612	4.387
(20, 40)	3.9482	0.9745
(50, 100)	3.7263	0.1515
(100, 200)	1.5870	0.0383

media to k_R (in the area of the resulting field). How do we form the incident wave in equations (2.57) – (2.60)?

The analytical definition of the incident wave in these expressions leads to a significant increase in errors [35] (Table 2.4, column a), compared with experiments in free space (Table 2.3) also as a result of the of non-compliance with the initial condition for the new phase difference of the incident wave between k_L and k_R. By moving the node k_R to the left to the disappearance of this phase difference we can improve the accuracy to a certain extent [35]. However, the study of the optical element does not yield information on the phase shift – it is part of the solution of the problem of diffraction at DOE.

Combining the numerical task of the incident wave (at the nodes k_L– 0.5 and k_L; the auxiliary problem is solved for the medium – a homogeneous dielectric) with the analytical task (at the nodes k_R and k_R+0.5) does not lead to a steady reduction of errors due to the influence of the analytical task in the right nodes for the whole computational domain [35].

The phase difference between the nodes k_L and k_R can be considered by assuming that the incident wave is not represented by the values of the domains of the second problem is k_R and k_R+0.5, and instead it is represented by the nodes that are separated from the data to the appropriate distance to the left (the wave velocity in a vacuum is higher than in a dielectric).However, this view does not account for the difference in phase shift in vacuum (main problem) and the dielectric (auxiliary problem) between i_R and i_R+0.5, which leads to an even greater decrease in accuracy. Making amendments to the analytical phase shift corresponds to the analytical task of the incident wave in the right nodes (i_R and i_R+0.5), discussed above.

Offering a solution to this problem, in this chapter we study the propagation of the field in a vacuum with the source (2.54), and this third problem is solved simultaneously with the two problems given in [35]. Thus, the value of the incident wave for the main problem (drop at the interface between the dielectric / vacuum) is substituted into equation (2.57), (2.58) of the second problem (which describes the propagation in a homogeneous dielectric), and in equations (2.59), (2.60) – for the third problem (propagation in free space). At the same time, to account for the

distance travelled by the wave in the first problem to the boundary between the two media, the values of the incident field are selected from the third problem not at the nodes k_R and k_R+0.5, but with a corresponding shift to the right.

As a result, we take into account numerically (not analytically) the phase difference of the waves between k_L and k_R, k_L–0. 5, and k_L, k_R and k_R+0.5, which improves the accuracy of numerical experiments (Table 2.4, column b).

The proposed method is characterized not only by solutions free from the spike of the values of the modulus of the complex amplitude in the right side of the computational domain, but does not limit the researcher in choosing the location of the site k_R. The initial condition for the numerical formulation of the radiating condition is always satisfied by virtue of its compliance with the two auxiliary problems (second and third).

Disadvantages of this approach includes an increase in computational complexity as a result of adding an additional one-dimensional problem. In the study of diffraction of a plane electromagnetic wave on two-dimensional and three-dimensional objects the indicated increase will not have any significant effect on the duration of the computation because of the dimensionaliyu of the added problem.

The two-dimensional case is characterized by the appearance of two new boundaries of separation parallel to the axis Z (Fig. 2.27 in [7]).

The grid subdomain of the resulting field is enclosed in the space between sections $j_T \le j \le j_B$, $k \le k_L$ (left boundary), $j_T \le j \le j_B$, $k \le k_R$ (right boundary), $j \le j_T$, $k_L \le k \le k_R$ (upper boundary), $j \le j_B$, $k_L \le k \le k_R$ (lower boundary), forming its boundaries.

For the separation of the resulting and scattered fields after the transition to the next temporal layer (for example, by (2.17) – (2.19)) we must carry out calculations:

$$H^{m+0.5}_{y_{j,k_L-0.5}} = H^{m+0.5}_{y_{j,k_L-0.5}} + \frac{h_t}{\mu_0 h_z}\tilde{E}^m_{x_{j,k_L}}, \tag{2.61}$$

$$H^{m+0.5}_{y_{j,k_R+0.5}} = H^{m+0.5}_{y_{j,k_R+0.5}} - \frac{h_t}{\mu_0 h_z}\tilde{E}^m_{x_{j,k_R}}, \tag{2.62}$$

$$E^{m+1}_{x_{j,k_L}} = E^{m+1}_{y_{j,k_L}} + \frac{h_t}{\varepsilon_0 \varepsilon_{j,k_L} h_z}\tilde{H}^{m+0.5}_{y_{j,k_L-0.5}}, \tag{2.63}$$

$$E^{m+1}_{x_{j,k_R}} = E^{m+1}_{y_{j,k_R}} - \frac{h_t}{\varepsilon_0 \varepsilon_{j,k_R} h_z}\tilde{H}^{m+0.5}_{y_{j,k_R+0.5}}, \tag{2.64}$$

$$H^{m+0.5}_{z_{j_T-0.5,k}} = H^{m+0.5}_{z_{j_T-0.5,k}} - \frac{h_t}{\mu_0 h_y}\tilde{E}^m_{x_{j_T,k}}, \tag{2.65}$$

$$H^{m+0.5}_{z_{j_B+0.5,k}} = H^{m+0.5}_{z_{j_B+0.5,k}} + \frac{h_t}{\mu_0 h_y}\tilde{E}^m_{x_{j_B,k}}, \tag{2.66}$$

$$E^{m+1}_{x_{j_T,k}} = E^{m+1}_{y_{j_T,k}} - \frac{h_t}{\varepsilon_0 \varepsilon_{j_T,k} h_z}\tilde{H}^{m+0.5}_{y_{j_T-0.5,k}}, \tag{2.67}$$